Breitenbach, S. F., Plessen, B., Waltgenbach, S., Tjallingii, R., Leonhardt, J., Jochum, K. P., Meyer, H., Goswami, B., Marwan, N., Scholz, D. (2019): Holocene interaction of maritime and continental climate in Central Europe: New speleothem evidence from Central Germany. - *Global and Planetary Change*, *176*, pp. 144–161.

DOI: http://doi.org/10.1016/j.gloplacha.2019.03.007

Holocene interaction of maritime and continental climate in Central Europe: new speleothem evidence from Central Germany

Sebastian F.M. Breitenbach[1,*], Birgit Plessen[2], Sarah Waltgenbach[3], Rik Tjallingii[2], Jens Leonhardt[4], Klaus Peter Jochum[5], Hanno Meyer[6], Bedartha Goswami[7], Norbert Marwan[7], Denis Scholz[3]

[1] Sediment- and Isotope Geology, Institute for Geology, Mineralogy and Geophysics, Ruhr-Universität Bochum, Universitätsstr. 150, 44801 Bochum, Germany
* sebastian.breitenbach@rub.de, phone: +49 23432 22307
[2] GFZ-Potsdam, Section Climate Dynamics and Landscape Evolution, Potsdam, Germany
[3] Institut für Geowissenschaften, Johannes Gutenberg-Universität, Mainz, Germany
[4] Thüringer Höhlenverein, Erfurt, Germany
[5] Climate Geochemistry Department, Max Planck Institute for Chemistry, Mainz, Germany
[6] Alfred Wegener Institute, Helmholtz Centre for Polar and Marine Research, Periglacial Research Section, Potsdam, Germany
[7] Potsdam Institute for Climate Impact Research (PIK), Member of the Leibniz Association, Potsdam, Germany

Abstract

Central European climate is strongly influenced by North Atlantic (Westerlies) and Siberian High circulation patterns, which govern precipitation and temperature dynamics and induce heterogeneous climatic conditions, with distinct boundaries between climate zones. These climate boundaries are not stationary and shift geographically, depending on long-term atmospheric conditions. So far, little is known about past shifts of these climate boundaries and the local to regional environmental response prior to the instrumental era.

High resolution multi-proxy data (stable oxygen and carbon isotope ratios, S/Ca and Sr/Ca) from two Holocene stalagmites from Bleßberg Cave (Thuringia) are used here to differentiate local and pan-regional environmental and climatic conditions Central Germany through the Holocene. Carbon isotope and S/Ca and Sr/Ca ratios inform us on local Holocene environmental changes in and around the cave, while $\delta^{18}O$ (when combined with independent records) serves as proxy for (pan-)regional atmospheric conditions.

The stable carbon isotope record suggests repeated changes in vegetation density (open vs. dense forest), and increasing forest cover in the late Holocene. Concurrently, decreasing S/Ca values indicate more effective sulphur retention in better developed soils, with a stabilization in the mid-Holocene. This goes in hand with changes in effective summer infiltration, reflected in the Sr/Ca profile. Highest Sr/Ca values between 4 ka and 1 ka BP indicate intensified prior calcite precipitation resulting from reduced effective moisture supply.

The region of Bleßberg Cave is sensitive to shifts of the boundary between maritime (Cfb) and continental (Dfb) climate and ideally suited to reconstruct past meridional shifts of this divide. We combined the Bleßberg Cave $\delta^{18}O$ time series with $\delta^{18}O$ data from Bunker Cave (western Germany) and a North Atlantic Oscillation (NAO) record from lake SS1220 (SW Greenland) to reconstruct the mean position of the Cfb-Dfb climate boundary. We further estimate the dynamic interplay of the North Atlantic Oscillation and the Siberian High and their influence on Central European climate. Repeated shifts of the Cfb-Dfb boundary over the last 4,000 years might explain previously observed discrepancies between proxy records from Europe. Detailed correlation analyses reveal multi-centennial scale alternations of maritime and continental climate and, concurrently, waning and waxing influences of Siberian High and NAO on Central Europe.

Keywords

Germany, Speleothem, Holocene, oxygen isotopes, carbon isotopes, S/Ca, Sr/Ca, palaeoclimate, continental climate, maritime climate, climate boundary

1. Introduction

European climate is characterized by heterogeneous climate conditions, with distinct boundaries that demarcate large-scale geographical regions with a coherent climatic pattern (Kottek et al. 2006). The coherence between the climatic characteristics within each such climate zone depends on large scale atmospheric systems and can be detected using climate network techniques (Rheinwalt et al. 2016). Central European climate is strongly influenced by intricately linked North Atlantic Oscillation (NAO) and Siberian High (SH), which govern (winter) precipitation and temperature over Europe. Both, NAO and SH, are expressions of (mainly winterly) semi-permanent, quasi-stationary surface pressure features that reside over the North Atlantic and northern Eurasia that closely interact with each other (Cohen et al. 2001). We will illuminate the non-stationary interaction between NAO and SH and its relation to the boundary that separates maritime and continental climates in the discussion below.

The boundary between the modern maritime Cfb and continental Dfb climatic zones according to the Köppen-Geiger classification (Peel et al. 2007), is not stationary, but shift in space and time (Kottek et al. 2006). Future shifts of the Cfb-Dfb climatic boundary mirror circulation changes that result from global warming and might lead to more frequent extreme weather patterns like heat waves and droughts, with significant repercussions for society (Cohen et al. 2014, Mann et al. 2018). To delineate the mechanisms related to Central European climate, it is imperative to understand the interaction of maritime and continental climates and the positioning of the border between the two. Climatic changes from multi-annual to centennial timescales can affect human society (Büntgen et al. 2011, 2016; Kennett & Breitenbach et al. 2012; Ludlow et al. 2013; Tan et al. 2015). Pre-industrial communities experienced spatio-temporal variations in regional precipitation and temperature (droughts, floods, unusual cold spells) more severely due to the direct impact on agricultural yield, in combination with high production and re-distribution costs. While multiple underlying causes for temperature or precipitation changes have been invoked, including solar and volcanic forcing, coupled with changes in atmospheric circulation patterns (Hurrell et al. 1995, Brönnimann et al. 2007, Ludlow et al. 2013, Ridley et al. 2015, Thieblemont et al. 2015, Büntgen et al. 2016), little is known about the associated changes in seasonal climate hydrological and thermal conditions in Central Europe for the Holocene (Simonis et al. 2012).

Temporally highly resolved (i.e. seasonal to decadal) multi-proxy climate reconstructions are the most promising tool to put the local and regional environmental response into perspective to global changes, including rising temperatures. Most importantly, there is an urgent need for palaeoclimate reconstructions, which are sensitive to seasonal aspects of regional and local climate as well as environmental conditions (Wong & Breeker 2015, James et al. 2015, Rehfeld et al. 2016). Only with sufficiently high resolved and spatially distributed reconstructions can we begin to quantify shifts in climate boundaries (Seager et al. 2018). Holocene climatic and environmental variability in Central Europe (and the responsible forcings) remains insufficiently understood, due to seasonal biases in some palaeoclimate time series, and a lack of chronological control in others. Although tree ring records give very detailed insights into changes in summer temperatures and precipitation, they cover only the last ~2.5 ka (Büntgen et al. 2006, 2011). Available high-resolution lacustrine reconstructions, based on robust varve counting and/or radiocarbon chronologies, often cover only parts of the Holocene (e.g. von Grafenstein et al. 1999, Martin-Puertas et al. 2012, Czymcik et al. 2016, Malkiewicz et al. 2016).

Speleothems (secondary cave carbonates) constitute powerful palaeo-environmental archives that can be dated very accurately radiometrically and provide a large number of environmental and climate proxies (Dorale et al. 2007, Fairchild & Baker 2012). However, so far, only a few speleothem-based Holocene records are available from Europe, mainly from southern and western Europe (Fohlmeister et al. 2012, Frisia et al. 2005a, McDermott et al. 2011, Mischel et al. 2017, Niggemann et al. 2003, Smith et al. 2016, Verheyden et al. 2000). One exception is the well dated high-resolution isotope record from Spannagel Cave, but due to its position in the Alps, it remains difficult to separate the influencing factors involved (Mangini et al. 2005, Fohlmeister et al. 2013). Highly resolved, well-dated time series are available, but limited to the last few thousand years (e.g. Proctor et al. 2000, Boch et al. 2009, Mangini et al. 2005). While these time series have added important details to our understanding of the factors that regulate European climate variability, additional spatial coverage is required to fully comprehend local to regional variability.

Here we present a multi-decadally to decadally resolved Holocene multi-proxy reconstruction from two stalagmites from Bleßberg Cave, Thuringia, Germany, and investigate shifts of the mean position of the maritime-continental climate boundary through time. The location of Bleßberg Cave at the western limit of continental climate region makes this study site particularly well suited to investigate spatio-temporal changes of the Cfb-Dfb boundary. $\delta^{13}C$ and $\delta^{18}O$ are combined with S/Ca and Sr/Ca records to gain insights into past local and (pan-)regional environmental dynamics in Central Europe over the last 11,000 years. We attempt to single out environmental responses to climatic changes at a more continental setting and to reconcile apparently divergent palaeoclimate reconstructions from different European regions. We argue that east-west shifting of the maritime and continental climate boundary might explain observed differences between palaeoclimate reconstructions from western and eastern sites. Our results suggest that reconstructions from western sites might not be representative of conditions further east and *vice versa* and that time series networks are needed to better understand local responses to global climatic changes.

2. Geographic and geologic setting

2.1 Geology and geography of Bleßberg Cave

The NW-SE oriented Bleßberg Cave is located at 50°25'28" N and 11°01'13" E at ca. 500 m a.s.l. at the southern fringe of the Thuringian schist mountains ca. 7 km from the town of Eisfeld, Germany (Fig. 1). Bleßberg Cave developed in Triassic marly limestones (Lower Muschelkalk/Anisium) and is orientated parallel to the Franconian Line, a Hercynian (NW-SE) directed, deep-reaching Cretaceous reverse fault (Reicherter et al. 2008). The cave was discovered in 2008 during construction of the new high-speed rail line between Berlin and Munich. Blasting work opened the cave ~240 m from the south portal of the ~8 km long Bleßberg tunnel.

The cave had no naturally accessible entrance prior to its discovery, but is drained by a small stream. The lack of a natural entrance preserved the cave from human or animal disturbance before 2008. The cave´s atmosphere is relatively stable, but the stream running through the main passage and airflow through breakdown could influence cave ventilation.

Bleßberg Cave is overlain by 12 to 50 m (35-40 m above the sampling site) of marly limestone (Lower and Middle Muschelkalk), which carries a relatively thin soil. The soil can be classified as agriculturally altered Leptosol (Rendzina, Ap-Ah-(T)-Cv-Cn, Boden AG 2006), possibly with clay enrichment below the Ah horizon. The vegetation directly above the cave is anthropogenically altered farmland, consisting mainly of weeds and crops, whereas uphill, mixed deciduous and pine forests take over.

2.2 Climatic characterization of the study site

The cave site is located near the watersheds between Weser, Elbe and Rhine rivers. Modern climate can be characterized as Cfb climate in the Köppen classification, with a mean annual air temperature of ca. 6°C at Neuhaus am Rennweg, ca. 12 km NE from the cave (Kottek et al. 2006). Rather high precipitation (862 mm/year, DWD Climate Data Center, www.dwd.de/EN/ourservices/cdcftp/cdcftp.html) results from orographic precipitation on the southwest-facing slope of the Thuringian mountains. Meteorological data from the station Neuhaus am Rennweg shows no significant seasonality in precipitation, whereas air temperature is highest in July (average T_{Jul} = 14.6°C) and coldest in January (average T_{Jan} = -3.2°C) (Fig. 2).

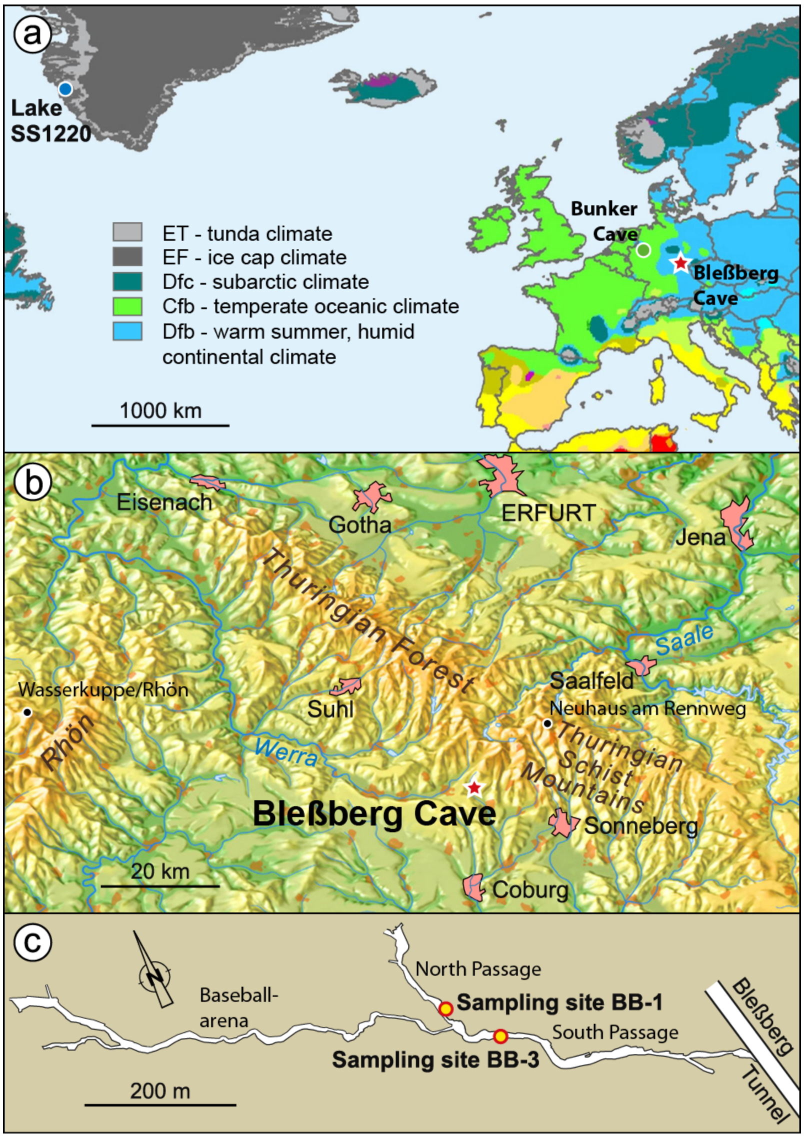

Figure 1: A) Location of Bleßberg Cave (red circle) in Central Europe. Bunker Cave and lake SS1220 in Greenland are shown as green star and blue circle respectively. Color coding indicates climate regimes according to Peel et al. (2007). The boundary between Cfb and Dfb climates crosses Central Europe meridionally. B) The study site is located at the SW facing slope of the Thuringian Schist Mountains near Eisfeld. The 2.5D elevation panorama has kindly been provided by mr-kartographie, Gotha, and is subject to copyright. C) Bleßberg Cave is oriented NW-SE, parallel to the Franconian Line, and was discovered during construction of the Bleßberg railway tunnel. The sampling sites are roughly in the middle of the poorly ventilated cave.

The seasonality in temperature leads to significant variation in potential and real evapotranspiration, which in turn leads to maximum effective infiltration between September and March (Fig. 2). Thus, the isotopic composition of dripwater entering Bleßberg Cave should be slightly biased towards the winter season, with implications for the interpretation of the $\delta^{18}O_{speleothem}$ signal, similar to other caves in Germany (e.g. Wackerbarth et al. 2010, Mischel et al. 2015).

Observational rainfall and temperature data reveals that winter temperature at Neuhaus am Rennweg correlates positively with the NAO index (data from ftp://ftp.cpc.ncep.noaa.gov), which is in agreement with the results of Baldini et al. (2008). The modern location of the Cfb-Dfb boundary east of Bleßberg Cave mirrors the oceanic influence in Central Europe (Kottek et al. 2006). In line with earlier results (Baldini et al. 2008, Riechelmann et al. 2017), we are confident that $\delta^{18}O$ in dripwater and speleothems can be used to study winter climate when the site is influenced by the Siberian High, which brings cold and dry air masses to Bleßberg Cave. The position of the cave near the western limit of the continental Dfb climate regime makes it highly sensitive to shifts of the boundary between the Cfb and the Dfb climate further west.

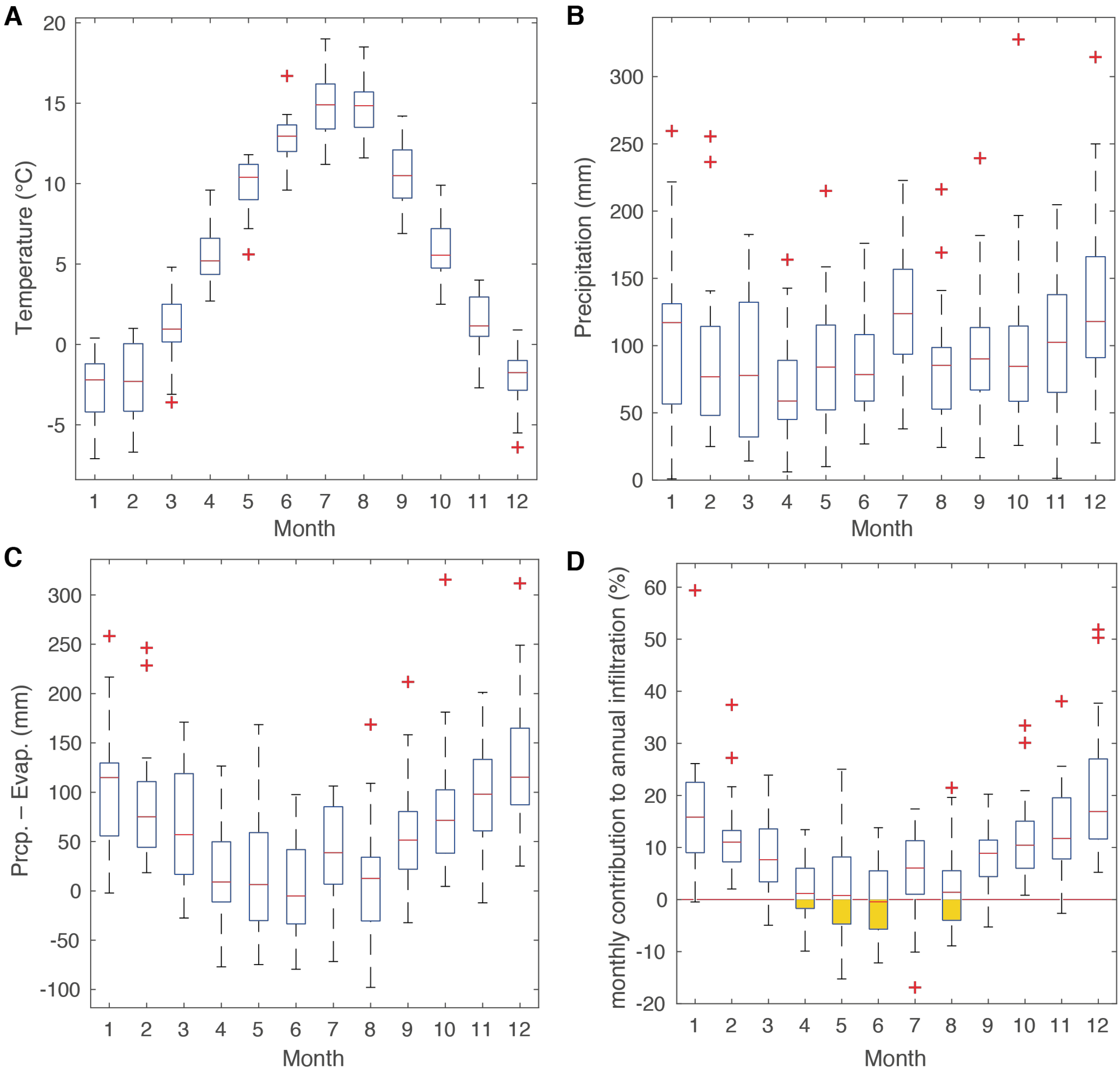

Figure 2: Boxplots of main meteorological characteristics at station Neuhaus am Rennweg. A) A clear seasonality, with maximum in summer is found in monthly temperature, B) monthly precipitation shows no distinct seasonal variability, C) monthly effective precipitation (precipitation minus potential evapotranspiration after Haude 1954) with maximum infiltration in winter, and D) monthly effective infiltration in percent of annual infiltration. Negative interquartile ranges are shown in yellow. The dataset includes the interval 31.05.1989 to 31.12.2014. Source: DWD climate data center.

This position however also means that any link between Bleßberg and the NAO system might be lost if the climate boundary is located west of the cave and continental climate prevails (see discussion).

2.3 Samples

The stalagmite samples BB-1 and BB-3 were recovered following the discovery of the cave. Sample BB-1 is 17.7 cm long and ca. 7 cm wide, while BB-3 is ca. 15 cm long with a diameter of ca. 9 cm. BB-1 was broken before collection, and the original drip site feeding this sample is thus unknown. Sample BB-3 was collected from the main passage and showed a fresh and wet surface (Fig. 1c). The samples were cut along their growth axes and polished and show a very clear, pale-ochre color, with rarely visible lamination and very little detrital material.

3. Methodology

3.1 Cave monitoring

In order to gain insight into cave ventilation and infiltration dynamics, which influence the geochemical proxies in Bleßberg Cave, microclimatic parameters are monitored. Between 2009 and 2012, monitoring was severely limited; since January 2013, data collection improved with renewed access to the cave. A CORA device (Luetscher & Ziegler 2012) is used to log temperature, humidity, air pressure and pCO_2 at 4-hour intervals. Dripwater was collected in airtight 5-12 mL vials during our visits and stored in cool, dark conditions until analysis. Stable isotope values ($\delta^{18}O$ and δD) of dripwater were determined at the Alfred Wegener Institute (AWI) in Potsdam. 18 samples were collected to cover the different seasons (Table 1, Fig. 3). A Finnigan MAT Delta-S mass spectrometer equipped with two equilibration units was used for the online determination of hydrogen and oxygen isotopic composition. The external errors for standard measurements of hydrogen and oxygen are better than 0.8‰ and 0.1‰, respectively (Meyer et al. 2000).

3.2 Mineralogy and geochemistry

Optical microscopy and fluorescence microscopy were performed on a Zeiss Jenalumar, SEM imaging and X-ray diffraction (XRD) at the Helmholtz Centre Potsdam, Deutsches GeoForschungsZentrum, Potsdam, Germany, to verify the mineral structure and lamination of the stalagmite samples. BB-1 consists of calcite and has been tested with cathodoluminescence (CL) microscopy to test for any diagenetic alterations. BB-3 grew on a flowstone in the middle of a ca. 8 m high passage and consists of calcite, too. Most of the stalagmite shows very clear parallel calcite crystals and horizontal growth layers, making the stalagmite ideally suited for palaeoclimate studies. The lowermost centimeters of the sample are already part of the underlying flowstone and show brownish clay layers and radial fan-structured crystals. Examination of thin sections under blue light reveals growth intervals with bright green laminae, suggesting the presence of organic material (Fig. 4b).

3.3 ^{230}Th/U dating

For ^{230}Th/U-dating, sub-samples with masses between 50 and 200 mg were cut from the growth axes of the individual stalagmites using a precision diamond wire saw as well as a micro band saw. In total, 41 ^{230}Th/U-ages were determined ($N_{BB\text{-}1}$ = 18, $N_{BB\text{-}3}$ = 23, Table 2). Chemical preparation and mass spectrometric analysis were performed at the Max Planck Institute for Chemistry, Mainz. For separation of Th and U, the samples were dissolved in 7N HNO_3, and a mixed ^{229}Th-^{233}U-^{236}U spike was added (see Gibert et al., 2016, for a detailed description of spike calibration). Potential organic material was removed by addition of a mixture of concentrated HNO_3, HCl and H_2O_2. After evaporation and re-dissolution in 6N HCl, U and Th were chemically separated using ion exchange column chemistry (Yang et al., 2015). For mass spectrometric measurements, the separated fractions of U and Th were dissolved in 2 ml of 0.8N HNO_3 and analysed with a Nu Plasma multi-collector inductively coupled plasma mass spectrometer (MC-ICPMS). Analytical details are described in Obert et al. (2016). Ages were calculated using the half-lives of Cheng et al. (2000), and the correction for potential detrital contamination assumes an average ^{232}Th/^{238}U weight ratio of the upper continental crust (3.8±1.9) and ^{230}Th, ^{234}U and ^{238}U in secular equilibrium.

Age-depth models for stable isotope and XRF proxy profiles were established using COPRA (Breitenbach et al. 2012). In order to calculate 2.5% and 97.5% quantile confidence limits (ca. 2σ), 5000 Monte Carlo (MC) simulations were run using a piecewise cubic interpolating. COPRA transposes the chronological uncertainty to the proxy domain, so that the x-axis (time) is error-free (Breitenbach et al. 2012). This procedure allows statistical reanalysis with the entire ensemble of age models.

3.4 Stable carbon and oxygen isotope analysis

Stable carbon and oxygen isotope ratios of the stalagmites (δ^{13}C and δ^{18}O) were determined at the Helmholtz-Centre Potsdam (GFZ). Stable isotope samples have been obtained using a “Sherline 5410” vertical milling machine with an inhouse-built sample stage and a micrometer-drive to allow precise movement of the speleothem block, for stepwise milling at a resolution of 0.1 mm. Carbonate aliquots were analysed for δ^{13}C and δ^{18}O values using a Finnigan MAT253 isotope ratio mass spectrometer (ThermoFisher Scientific) connected to an automated carbonate-reaction device (KIEL IV). Samples of around 20-60 µg were automatically dissolved with 103% H_3PO_4 at 72°C, and the isotopic composition was measured on the released and cryogenically purified CO_2. Results are reported relative to VPDB, and replicate analysis of international reference material (NBS19) yielded external standard deviations of 0.06 ‰ (1σ) for both δ^{13}C and δ^{18}O.

3.5 Micro-XRF analysis

The distribution of elements detectable with micro X-ray fluorescence (µXRF) has been determined in both samples, BB-1 and BB-3 (Figs. 4a, b). Both samples were scanned along the stable isotope track using an EAGLE III XL µXRF spectrometer (Röntgenanalytik, Germany) at the GFZ. The µXRF is equipped with a 50 W Rh X-ray source that was operated at 40kV and 300 µA. Measurements were performed under vacuum every 40 µm with a spot size of 50 µm and a counting time of 60 s. The resulting intensities are given in counts per second (cps) and the reproducibility is proven with repeated measurements. Besides Ca, significant count variations were found for Sr and S. Element intensities have been normalized over Ca to minimize sample density effects and scaled by multiplying the intensity ratios by 1000.

4. Results

4.1 Cave microclimate monitoring

Bleßberg Cave has a rather stable thermal regime, with a mean temperature of 8.7±0.1°C and a relative humidity of 99.8±0.2 %. Cave air pCO_2 is slightly elevated relative to outside air and varies from 780 to 824 ppm, with a maximum in winter, which probably results from enhanced effective infiltration and introduction of soil CO_2 in winter. Although the level of the cave stream changes significantly in the eastern cave passages, it seems not to strongly alter the cave atmospheric conditions.

Stable oxygen and deuterium isotope values (Table 1) from 18 Bleßberg Cave dripwater samples are relatively invariable, with δD = -65.5±1.7‰ and $\delta^{18}O$ = -9.5±0.2‰ (Fig. 3a) and agree well with the winter season (Sep-Mar) averages of precipitation from GNIP stations Wasserkuppe/Rhön ($\delta D_{Sep\text{-}Mar}$ = -69.6‰, $\delta^{18}O_{Sep\text{-}Mar}$ = -10.1±1‰, IAEA/WMO 2017), Hof ($\delta D_{Sep\text{-}Mar}$ = -71.3‰, $\delta^{18}O_{Sep\text{-}Mar}$ = -9.8±1.3‰) and Leipzig ($\delta D_{Sep\text{-}Mar}$ = -67.1‰, $\delta^{18}O_{Sep\text{-}Mar}$ = -9.6±1.4‰) (Figs. 3a, b, IAEA/WMO 2017; meteorological data cover 1983-2003 for Hof and Wasserkuppe/Rhön, and 1986-2003 for Leipzig). The slightly lower mean winter value for Wasserkuppe/Rhön is due to the altitude effect (the station's altitude is 921 m a.s.l., compared to 567 m in Hof and 125 m in Leipzig). All values fall on the Global Meteoric Water Line (GMWL, Fig. 3b), which indicates that no secondary evaporation effects influence our samples. The d excess is in the range of global average of precipitation. Temporal and spatial dripwater $\delta^{18}O$ variability is rather small, with only about 0.6 ‰ variation between different sampling days and sampling spots in different cave passages, but denser sampling is needed to evaluate this aspect.

4.2 $^{230}Th/U$ dating and age modeling

The results of $^{230}Th/U$-dating are presented in Table 2. The ^{238}U concentration of the stalagmites varies between 0.614±0.009 (BB-3) and 3.74±0.02 µg g^{-1} (BB-1). BB-1 has a substantially higher ^{238}U-concentration compared to BB-3. The ^{232}Th-concentration is generally low (<1 ng g^{-1}; Table 2) and even below the detection limit for some samples.

Only four samples show an elevated input of detrital material with a ^{232}Th-content between 1.09±0.01 ng g^{-1} (NR-31 of BB-1) and 55.87±0.53 ng g^{-1} (BB3-5.2 of BB-3), respectively. All four samples were taken at the base of the two stalagmites. The relatively high concentrations of uranium (up to 3.4 μg/g) and lack of detrital thorium (Table 2) result in mean dating errors of ±30 years in BB-1 and ±86 years in BB-3 (2σ).

Stalagmite BB-1 grew between 5.6 and 0.6 ka BP (kilo years before present, i.e. 1950 CE), while BB-3 grew between 11.9 and 5.4 ka BP (Fig. 5). Unfortunately, the last ca. 600 years are missing and the reconstruction cannot be directly linked with meteorological data.

The age-depth slopes indicate that both stalagmites grew at different rates; slow growth prevailed between ca. 11 and 7 ka BP and 3.7 and 0.2 ka BP, whereas faster growth occurred in the mid-Holocene between 6 and 4 ka BP (Fig. 5). BB-3 shows relatively steady growth in the early Holocene and a slight increase after ca. 7 ka BP. A hiatus has been identified during ^{230}Th/U-dating of BB-3, located at 100.2 mm from top, which is characterized by yellow-brownish coloring of the stalagmite. This hiatus covers a ca. 400-year long interval between 8.26 and 7.85 ka BP. BB-1 shows a drastic reduction in growth rate after ca. 4.7 ka BP, approaching values more similar to those in the early Holocene. While growth rates differ, the convergence in both stalagmites during the overlapping period suggests common forcing(s) that adjust the growth pattern. The interval where both stalagmites overlap (ca. 5.6 to 5.2 ka BP) reveals that BB-3 (the older of the two) has lower δ^{13}C and S/Ca, and higher Sr/Ca and δ^{18}O values compared to BB-3. BB-1 also shows higher high-frequency variability.

Table 1 Dripwater samples collected in Bleßberg Cave for stable isotope analysis.

Sample ID	Sampling date	Location	δ^{18}O [‰ VSMOW]	δ^{2}H [‰ VSMOW]	d excess
BBH-NG-23.01.09	23.01.2009	N. Passage	-9.61	no data	no data
BBH-NG-23.01.09	23.01.2009	N. Passage	-9.62	-65.2	11.7
BBH-NG-23.01.09	23.01.2009	N. Passage	-9.59	-66.1	10.6
BBH-SG-24.01.09	24.01.2009	S. Passage	-9.11	-61.6	11.3
BBH-SG-24.01.09	24.01.2009	S. Passage	-9.13	NAN	NAN
BBH-SG-24.01.09	24.01.2009	S. Passage	-9.11	-61.6	11.3
BBH-MP1 24.11.2012	24.11.2012	Station 1	-9.72	-66.9	10.9
BBH-MP2 24.11.2012	24.11.2012	Station 1	-9.72	-66.6	11.2
dripwater 24.08.2013 BB-1	24.08.2013	S. Passage	-9.71	-67.3	10.4
dripwater 24.08.2013 BB-1	24.08.2013	S. Passage	-9.64	-66.7	10.4
dripwater 24.08.2013 86	24.08.2013	S. Passage	-9.67	-66.7	10.7
dripwater 24.08.2013 2m 86	24.08.2013	S. Passage	-9.20	-64.9	8.7
drip water 24.08.2013 103	24.08.2013	S. Passage	-9.56	-66.1	10.4
drip water 24.08.2013 2m 103	24.08.2013	S. Passage	-9.52	-66.0	10.2
drip water 27.05.2017, MP90	27.05.2017	Baseball Arena	-9.63	-64.9	12.2
drip water 27.05.2017, MP90	27.05.2017	Baseball Arena	-9.42	-64.6	10.8
drip water 27.05.2017, MP90	27.05.2017	Baseball Arena	-9.58	-64.6	12.1
drip water 27.05.2017, MP90	27.05.2017	Baseball Arena	-9.67	-64.6	12.8

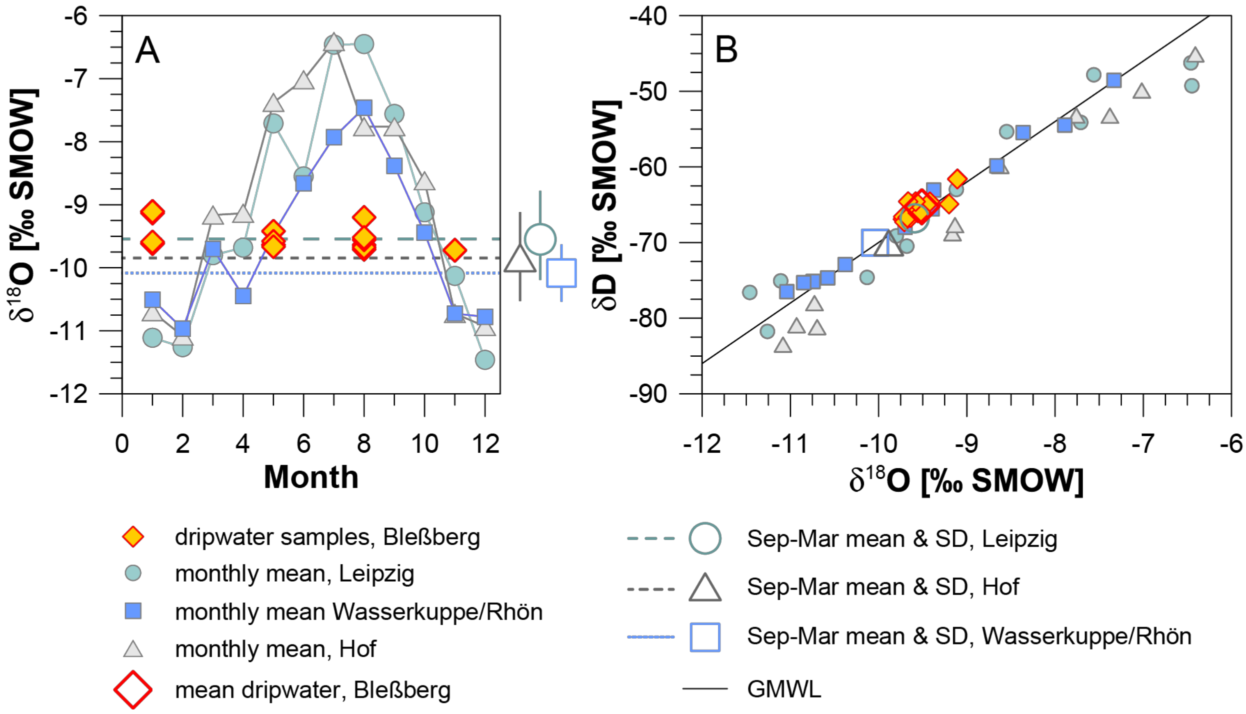

Figure 3: Stable isotope data from dripwater and precipitation. A) Dripwater $\delta^{18}O$ data from Bleßberg Cave compared with mean monthly $\delta^{18}O$ of precipitation at Wasserkuppe/Rhön (squares), Leipzig (circles) and Hof (triangles) (IAEA/WMO 2017). B) Cross-plot of dripwater and monthly mean precipitation $\delta^{18}O$ and δD values from the same stations. Large empty symbols denote mean values for the winter season (September to March).

Before an interpretation in terms of environmental changes can be attempted the observed offsets must be explained as both stalagmites are apparently precipitated from different feeding systems. BB-1 was likely fed from fracture flow, whereas BB-3 received seepage flow water from a low-permeability host rock matrix (Fairchild and McMillan 2007).

Seepage flow from the epikarst matrix goes in hand with prolonged residence time of infiltrating water and mixing of waters of different age. This ultimately leads to smoothing of the proxy signals, which explains the reduced high-frequency variability in BB-3. Seepage flow from a less permeable matrix forces longer interaction of the infiltrating water with soil and host rock, which can well explain the observed lower $\delta^{13}C$ and S/Ca ratios, and higher Sr/Ca levels in BB-3. Lower $\delta^{13}C$ in BB-3 compared to BB-1 can be explained by less CO_2-degassing in a matrix with lower permeability, i.e. seepage from a host rock matrix is less prone to open conditions and PCP, compared to fracture flow where open conditions might occur faster and more frequently (Fairchild and McMillan 2007). Lower S/Ca ratios in BB-3 might result from better sulfur retention in the host rock, compared to larger fractures. Prolonged dissolution of host rock in a seepage flow system can also increase the Sr/Ca baseline in BB-3 (which is subsequently modulated by PCP dynamics). On the other hand, a fracture-flow fed BB-1 would reflect a faster response to changes in infiltration, higher S/Ca caused by lower sulfur retention in the soil and epikarst, and a lower Sr/Ca baseline due to shorter water-rock interaction. Finally, the lower $\delta^{18}O$ values observed in BB-1 might result from a more direct response to cold-season infiltration and/or spring snowmelt through the fractures feeding BB-1, and less mixing with summer-season water in the epikarst. These factors must be kept in mind when interpreting the proxy variability in both stalagmite records. We note however that millennial-scale trends and centennial dynamics in both records are still interpretable in terms of environmental conditions at the cave site."

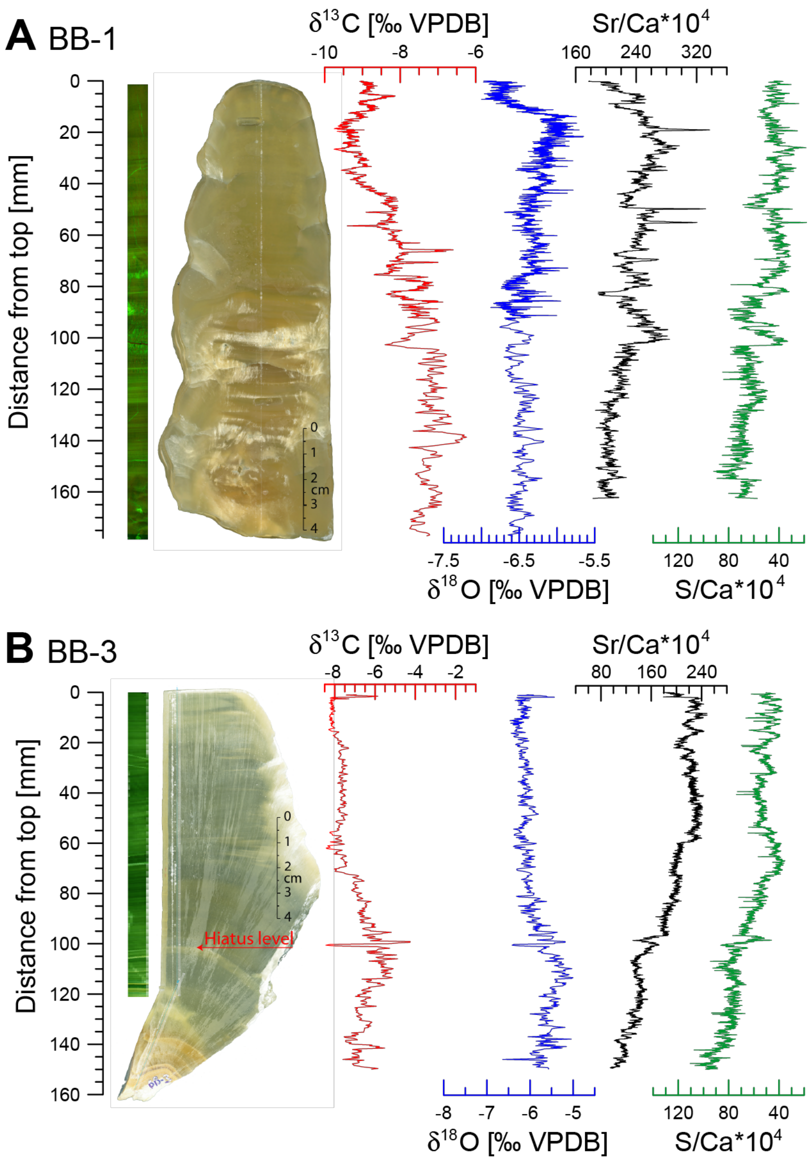

Figure 4: Images of stalagmites BB-1 (A) and BB-3 (B), together with fluorescence images, stable isotope profiles ($\delta^{13}C$ and $\delta^{18}O$) and µXRF Sr/Ca, and S/Ca ratios. The lower brownish section of BB-3 belongs genetically to the flowstone onto which BB-3 grew and the geochemical data from this interval is not discussed in the main text.

4.3 Stable isotopes

In total, about 2000 samples have been analysed for stable isotopes in both stalagmites (1451 in BB-1, and 538 in BB-3). The total amplitude in $\delta^{18}O$ across the entire Holocene is ~2‰, from −5‰ around 9 ka BP to −7‰ in the last millennium (Figs. 4a, 6). In the younger stalagmite BB-1, $\delta^{18}O$ values range from −7‰ to −5.7‰, with an increasing trend from ca. −6.5‰ in the lower part towards a maximum value of −5‰ at 1.3 ka BP. At the top, the BB-1 profile shows a large shift to values around −6.8‰. Superimposed on the millennial to centennial changes, multi-decadal variability is detected with amplitudes of 0.3 to 0.5‰. In the older stalagmite BB-3, $\delta^{18}O$ values vary from −8‰ to −5‰. A trend to lower values is observed in the upper half of this stalagmite (since ~9 ka BP), which is only interrupted by two prominent excursions before and after the hiatus around 8 ka BP. A first notable shift of ~0.8‰ to lower values occurred just before the hiatus. A second shift is found after the hiatus, with a rapid change from values around −5.4‰ to −6‰ (Figs. 4b, 6). No clear trend is found between 7.2 and 5.3 ka BP, but multi-centennial scale variability of ~0.2-0.4‰ characterizes this section. Where BB-3 overlaps with BB-1, it is offset and less negative by ~0.5‰.

Across both stalagmites, $\delta^{13}C$ values vary ~8.5‰, from −9.8‰ to −1‰ (Figs. 4, 6), with a general trend towards lower values through the Holocene (Fig. 6). A plateau, with values around −7‰, is found between 11 ka BP and 9 ka BP. This stable phase is interrupted at ~11 ka BP, when $\delta^{13}C$ increased about 1‰ for 400 years. Around 8.7 ka BP, a rapid 2‰ shift to more negative values occurred, followed by the hiatus (~8.3-7.8 ka BP). This hiatus lasted 400 years, after which growth commenced again. The $\delta^{13}C$ profile restarted with values around -6‰, decreasing steadily to −8‰ around 7 ka BP (Fig. 6). Variable $\delta^{13}C$ values are found during the mid-Holocene. After 3 ka BP, a further decrease occurred, with the lowest values of the entire profile at around 2 ka BP, and a last shift to higher values since 1.5 ka BP.

In addition to the samples obtained for proxy records, ~250 samples were drilled for Hendy tests (Hendy 1971). In BB-1, 5 Hendy test transects were performed, with 10 to 15 samples each. Neither a significant positive correlation between $\delta^{13}C$ and $\delta^{18}O$, nor an increase of $\delta^{18}O$ values with distance from the apex is observed. From BB-3, no Hendy tests have been obtained.

Table 2: Results of the ^{230}Th/U-dating. Activity ratios are indicated by parentheses.

Sample ID	Depth [mm]	^{238}U [µg g^{-1}]	^{232}Th [ng g^{-1}]	(^{234}U/^{238}U)	(^{230}Th/^{238}U)	(^{234}U/^{238}U)$_{initial}$	age$_{uncorrected}$ [ka BP]	age$_{corrected}$ [ka BP]
BB-1 17	5.00	1.772 ± 0.011	0.0334 ± 0.0018	2.5544 ± 0.0031	0.01546 ± 0.00026	2.5573 ± 0.0030	0.600 ± 0.011	0.599 ± 0.011
BB-1 25	13.75	2.240 ± 0.012	< LoD	2.5606 ± 0.0033	0.02956 ± 0.00048	2.5662 ± 0.0033	1.204 ± 0.020	1.204 ± 0.020
BB-1 18	22.00	2.145 ± 0.013	0.0431 ± 0.0013	2.5601 ± 0.0036	0.04076 ± 0.00034	2.5678 ± 0.0036	1.687 ± 0.015	1.687 ± 0.015
BB-1 1	27.00	1.789 ± 0.011	0.02200 ± 0.00087	2.5363 ± 0.0039	0.04755 ± 0.00045	2.5453 ± 0.0038	2.002 ± 0.020	2.202 ± 0.020
BB-1 26	38.00	2.254 ± 0.012	< LoD	2.5598 ± 0.0034	0.06263 ± 0.00050	2.5717 ± 0.0034	2.636 ± 0.023	2.636 ± 0.022
BB-1 19	46.00	2.480 ± 0.016	0.0552 ± 0.0019	2.6334 ± 0.0047	0.07322 ± 0.00071	2.6477 ± 0.0047	3.008 ± 0.031	3.008 ± 0.032
BB-1 9	50.75	2.330 ± 0.015	0.0501 ± 0.0013	2.6158 ± 0.0037	0.07996 ± 0.00055	2.6313 ± 0.0037	3.317 ± 0.024	3.317 ± 0.020
BB-1 20	64.00	2.424 ± 0.017	0.0350 ± 0.0011	2.5585 ± 0.0084	0.09154 ± 0.00060	2.5761 ± 0.0083	3.902 ± 0.030	3.902 ± 0.030
BB-1 27	69.00	2.448 ± 0.013	< LoD	2.5770 ± 0.0035	0.09779 ± 0.00076	2.5958 ± 0.0036	4.146 ± 0.033	4.146 ± 0.034
BB-1 28	73.00	2.332 ± 0.012	< LoD	2.5883 ± 0.0031	0.1036 ± 0.0015	2.6083 ± 0.0032	4.379 ± 0.067	4.379 ± 0.068
BB-1 10	75.75	2.838 ± 0.019	0.0588 ± 0.0016	2.5686 ± 0.0033	0.10590 ± 0.00081	2.5891 ± 0.0032	4.516 ± 0.035	4.516 ± 0.040
BB-1 21	84.00	2.235 ± 0.014	0.0879 ± 0.0017	2.6106 ± 0.0035	0.11064 ± 0.00057	2.6321 ± 0.0035	4.647 ± 0.025	4.646 ± 0.025
BB-1 29	93.75	3.489 ± 0.019	0.3223 ± 0.0062	2.5826 ± 0.0036	0.11276 ± 0.00092	2.6045 ± 0.0037	4.792 ± 0.041	4.791 ± 0.041
BB-1 30	107.00	3.739 ± 0.020	0.6705 ± 0.0087	2.5768 ± 0.0034	0.11429 ± 0.00077	2.5989 ± 0.0034	4.872 ± 0.034	4.870 ± 0.035
BB-1 2	119.50	3.146 ± 0.022	0.0953 ± 0.0016	2.6056 ± 0.0062	0.11809 ± 0.00064	2.6286 ± 0.0062	4.981 ± 0.031	5.981 ± 0.030
BB-1 11	137.00	3.445 ± 0.022	0.4939 ± 0.0056	2.6072 ± 0.0036	0.12344 ± 0.00068	2.6314 ± 0.0035	5.210 ± 0.030	5.209 ± 0.030
BB-1 3	153.50	3.153 ± 0.020	0.6703 ± 0.0073	2.6034 ± 0.0036	0.12683 ± 0.00063	2.6282 ± 0.0036	5.367 ± 0.029	5.365 ± 0.030
BB-1 31	170.25	3.489 ± 0.020	1.0871 ± 0.0140	2.5966 ± 0.0053	0.1305 ± 0.0010	2.6221 ± 0.0054	5.542 ± 0.045	5.539 ± 0.045
BB3-1	7.00	1.0058 ± 0.0052	0.00249 ± 0.00055	2.6449 ± 0.0029	0.12900 ± 0.00090	2.6703 ± 0.0029	5.370 ± 0.040	5.370 ± 0.039
BB3-3.1	13.00	1.1394 ± 0.0073	0.01789 ± 0.00092	2.628 ± 0.010	0.1311 ± 0.0010	2.654 ± 0.010	5.493 ± 0.049	5.493 ± 0.049
BB3-2.1	23.50	1.3399 ± 0.0077	0.01428 ± 0.00039	2.6977 ± 00.0086	0.1365 ± 0.0011	2.7250 ± 0.0084	5.577 ± 0.048	5.576 ± 0.047
BB3-2	41.50	1.4212 ± 0.0074	< LoD	2.7119 ± 0.0026	0.15060 ± 0.00087	2.7421 ± 0.0027	6.140 ± 0.038	6.140 ± 0.038
BB3-3.2	54.50	1.263 ± 0.010	0.02225 ± 0.00098	2.645 ± 0.017	0.1554 ± 0.0015	2.676 ± 0.016	6.508 ± 0.077	6.507 ± 0.076
BB3-3	68.50	0.9372 ± 0.0049	0.01793 ± 0.00057	2.6959 ± 0.0031	0.1634 ± 0.0010	2.7288 ± 0.0032	6.721 ± 0.042	6.721 ± 0.042
BB3-4.1	75.8	0.9140 ± 0.0050	0.0369 ± 0.0010	2.7006 ± 0.0037	0.1742 ± 0.0022	2.7357 ± 0.0037	7.168 ± 0.094	7.168 ± 0.095
BB3-4.2	85.3	0.8869 ± 0.0049	0.01965 ± 0.00083	2.6871 ± 0.0036	0.1782 ± 0.0026	2.7229 ± 0.0036	7.38 ± 0.11	7.38 ± 0.11
BB3-4.3	90.4	1.0252 ± 0.0055	0.02138 ± 0.00070	2.6986 ± 0.0031	0.1823 ± 0.0021	2.7354 ± 0.0031	7.520 ± 0.090	7.520 ± 0.090
BB3-4	93.3	0.9824 ± 0.0051	0.01449 ± 0.00060	2.6941 ± 0.0027	0.1857 ± 0.0012	2.7316 ± 0.0027	7.681 ± 0.049	7.680 ± 0.049
BB3-4.4	95.9	0.9500 ± 0.0051	0.02093 ± 0.00061	2.7095 ± 0.0032	0.1869 ± 0.0017	2.7474 ± 0.0033	7.685 ± 0.075	7.684 ± 0.075

BB3-4.5	97.8	0.6847 ± 0.0037	0.0813 ± 0.0019	2.7051 ± 0.0031	0.1883 ± 0.0025	2.7432 ± 0.0031	7.76 ± 0.10	7.76 ± 0.11
BB3-4.6	100.3	0.8475 ± 0.0046	0.0406 ± 0.0012	2.6870 ± 0.0032	0.2036 ± 0.0026	2.7282 ± 0.0033	8.54 ± 0.12	8.54 ± 0.12
BB3-4.7	102.9	0.8829 ± 0.0047	0.0458 ± 0.0011	2.6979 ± 0.0033	0.2069 ± 0.0019	2.7399 ± 0.0034	8.581 ± 0.083	8.580 ± 0.083
BB3-2.2	106.8	0.7950 ± 0.0047	0.03316 ± 0.00065	2.6958 ± 0.0092	0.2114 ± 0.0019	2.739 ± 0.010	8.781 ± 0.088	8.781 ± 0.087
BB3-5	112.50	0.6969 ± 0.0036	0.0794 ± 0.0011	2.7504 ± 0.0029	0.2227 ± 0.0012	2.7962 ± 0.0029	9.080 ± 0.052	9.079 ± 0.051
BB3-3.6	121.50	0.8424 ± 0.0064	0.0823 ± 0.0015	2.719 ± 0.015	0.2316 ± 0.0025	2.767 ± 0.015	9.57 ± 0.12	9.57 ± 0.13
BB3-6	124.50	0.7713 ± 0.0040	0.05218 ± 0.00092	2.7477 ± 0.0027	0.2361 ± 0.0014	2.7963 ± 0.0028	9.659 ± 0.058	9.658 ± 0.058
BB3-3.7	130.3	0.7511 ± 0.0085	0.1224 ± 0.0019	2.719 ± 0.027	0.2473 ± 0.0031	2.769 ± 0.028	10.25 ± 0.17	10.25 ± 0.17
BB3-2.3	133.3	0.7367 ± 0.0044	0.872 ± 0.013	2.758 ± 0.010	0.2519 ± 0.0032	2.810 ± 0.010	10.31 ± 0.14	10.29 ± 0.15
BB3-5.1	138.3	0.9239 ± 0.0053	13.45 ± 0.12	2.8869 ± 0.0081	0.2736 ± 0.0020	2.9451 ± 0.0081	10.839 ± 0.064	10.697 ± 0.087
BB3-7	141.00	0.7759 ± 0.0040	15.85 ± 0.15	2.9018 ± 0.0059	0.2867 ± 0.0023	2.9632 ± 0.0060	11.37 ± 0.056	11.17 ± 0.10
BB3-5.2	147.5	0.6155 ± 0.0036	55.87 ± 0.53	2.949 ± 0.025	0.3065 ± 0.0087	3.015 ± 0.025	12.665 ± 0.088	11.78 ± 0.37

LoD = Limit of Detection; BP = before present, i.e. 1950 CE

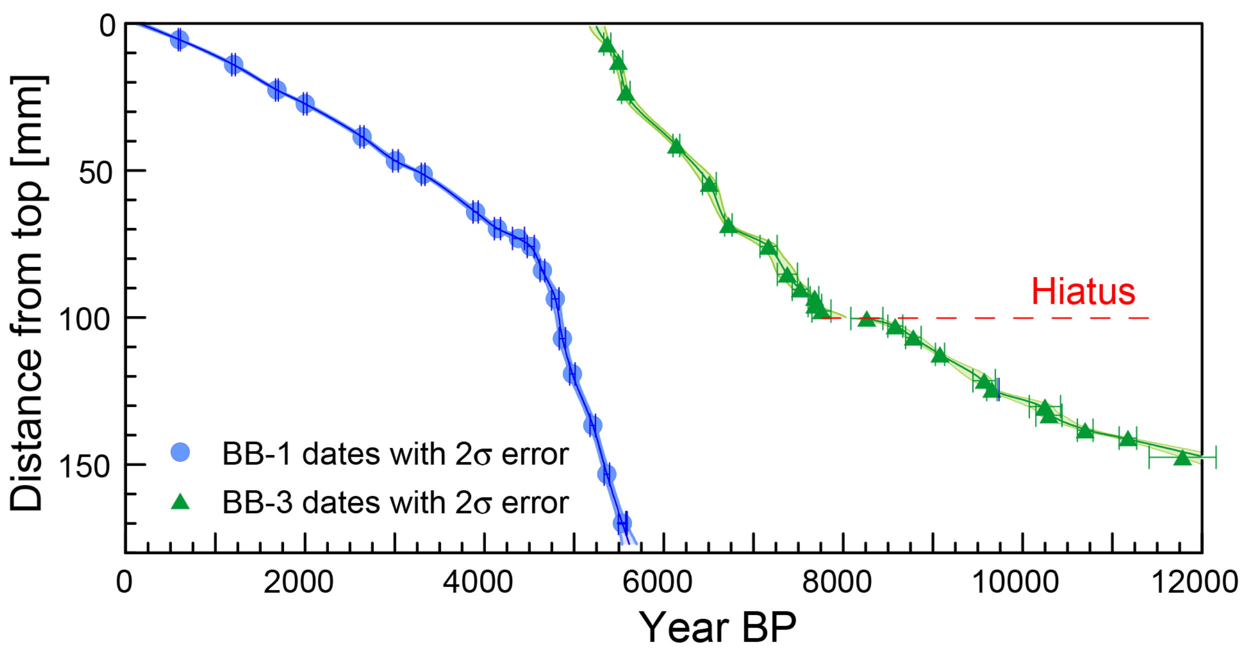

Figure 5: Age models for stalagmites BB-1 (blue) and BB-3 (green). Median growth and the 2.5% and 97.5% confidence envelopes are shown together with the individual ^{230}Th/U-ages and 2σ errors. The age models are based on 5000 Monte Carlo simulations and polynomial interpolation between the discrete dates.

4.4 µXRF data

In the older stalagmite BB-3, the Sr/Ca ratio varies from 65 and 160, while in BB-1, it ranges from 100 to 195 (Fig. 4). In BB-3, Sr/Ca increases slowly until ca. 6.8 ka BP, and reaches then a relatively stable level at ca. 150, before the values fall back to ca. 120 at the top of the stalagmite. The general trend varies only little. In BB-1, the Sr/Ca profile is characterized by a higher degree of variability. Starting at ca. 120, it increases to ca. 160 until ca. 3.3 ka BP, when the values drop to ca. 130. Afterwards, Sr/Ca values increase again until ca. 2 ka BP, before the trend reverses, and Sr/Ca values are lowest values in BB-1 (ca. 100). High-frequency changes are found superimposed on the long-term trends. Sharp multi-decadal increases are found at 4.8, 3.5, 3.2, and 1.5 ka BP, with Sr values reaching 195.

S/Ca ratios show a long term trend opposite to Sr/Ca over the Holocene. In BB-3, a multi-millennial trend to lower S/Ca values is found (Fig. 4c), from 80 in the early Holocene to 30 at around 6 ka BP. Few significant deviations are observed, although centennial-scale changes are present. In BB-1, S/Ca values further decline between 5.6 and 4.5 ka BP, but then stabilize at a level of 30 to 20 (Fig. 4a). Only minor fluctuations are observed at centennial scale, with one stronger shift to higher S/Ca values at 3.3 ka BP and a second possibly at 1.7 ka BP.

4.5 Statistical analyses of spatio-temporal relationships between proxy records

To statistically test for periods of east- and westward Cfb/Dfb boundary migration, we performed a rigorous correlation analysis on the δ^{18}O time series from BB-1 and BU-4 and the DSM record from lake SS1220. As the sampling resolution of the proxy records is different and irregular, and the time axes contain a certain amount of uncertainty, we use a special correlation analysis that considers the chronological uncertainties of each record when calculating correlations. For all palaeoclimate records, we consider a moving window of 500 years, moved in steps of 50 years over the time span 4 to 0.5 ka BP. At each window position the COPRA proxy record ensembles (with 5,000 members each) for the two caves are taken and in a first step 5,000 pairs of proxy records are randomly selected, one from each cave. For each pair, we extract the part of the proxy time series that falls within the time window, and estimate the cross-correlation at lag zero between these extracted sub-time series using a Gaussian kernel-based correlation approach (NESTool, normalised kernel width h = 0.75) (Rehfeld et al., 2011). This results in an empirical test distribution of 5,000 correlation estimates for that particular window location. Repeating this for all other timings of the window, we obtain an ensemble of 5,000 time series of correlation estimates. The statistical significance of this 'observed' correlation distribution is obtained on the basis of a 2-sample Kolmogorov-Smirnov (KS) test, which tests the null hypothesis that the probability distribution of the correlation samples (from the observed data) equals the probability distribution of correlation values of uncorrelated times series of the same statistical properties than the observed data). The random correlation estimates are obtained by repeating the correlation calculation as before, but with the difference that the randomly chosen proxy time series are further uniform-randomly shuffled before estimating the kernel-based cross correlation. The KS test statistic is based on the maximum difference between the two empirical cumulative distribution functions obtained from the two correlation samples and is not necessarily related to an overlap of their interquartile ranges. This test provides a p-value, the statistical significance of which is obtained at a confidence level of 1%, after taking into account multiple comparisons by using Holm's method combined with the Dunn–Šidák correction factor.

5. Discussion

Stable oxygen and carbon isotope data from speleothem carbonates have been studied for decades, but ambiguities remain with regard to identification of the processes underlying changes in these isotope proxy records (e.g. Gascoyne 1992, McDermott 2004, Mangini et al. 2005, Lachniet 2009, Fairchild & Baker 2012). To fully understand individual controls on environmentally sensitive proxies, monitoring is required at the local level. Here, the combination of stable isotope and µXRF elemental data allows detailed insights into seasonally-biased controls on the proxies in speleothems from Bleßberg Cave and the reconstruction of local and (pan-)regional environmental changes. Since the hydrological system in the epikarst acts as a low pass filter, the climatic signal does not reach the cave immediately, thus imposing a lag of unclear but likely annual to multiannual length to speleothem records from Bleßberg Cave

5.1 Interpretation of geochemical proxies

5.1.1 $\delta^{13}C$, S/Ca and Sr/Ca records as proxies for vegetation, soil development and infiltration

Both stalagmite $\delta^{13}C$ values and S/Ca ratios (Fig. 6a, b) can serve as proxy for changes in vegetation composition and density, soil microbial activity as well as changes in infiltration (Lechleitner et al. 2017). In temperate locations, these factors contribute most to the carbon budget in the dripwater and can be reflected in speleothem $\delta^{13}C$ values (Genty & Massault 1999; Genty et al. 2001; Fairchild & Baker 2012). Speleothem Sr/Ca constitutes a sensitive proxy for changes in infiltration, with higher values being recorded during times of reduced moisture availability (Fairchild & Treble 2009). Since Bleßberg Cave had no natural entrance before its discovery during tunnel construction, ventilation-induced in-cave CO_2 degassing can be regarded as subordinate process affecting the $\delta^{13}C$ values of the dissolved inorganic carbon (DIC) and in stalagmites. CO_2 dynamics could potentially be mediated by changing stream volume and/or flow velocity (Troester & White 1984). Unfortunately, in Bleßberg Cave, this process cannot be tested as a consequence of the massive concrete injection during the tunneling process (ILEK 2011).

The Bleßberg site is characterized by higher soil microbial and vegetation activity during spring and summer, which, together with higher winterly effective infiltration induces elevated (relative to surface atmosphere) CO_2 levels with low soil $\delta^{13}C$ signature. In the epikarst, this $\delta^{13}C$ signal is adjusted to more positive values, depending on the residence time of the percolating water, and ultimately transferred to the cave (Lechleitner et al. 2017). The stalagmites then record a complex signal of epikarst and in-cave degassing, vegetation composition and density as well as soil microbial activity above the cave (McDermott 2004). This mechanistic explanation is corroborated by the observed low $\delta^{13}C$ values between -7‰ and -10‰ in the time series from Bleßberg Cave. If $\delta^{13}C$ would solely reflect the composition of the host rock limestone much higher values (+1 to -2‰) would be expected. Thus, we infer that Holocene vegetation and soil development left a recognizable imprint on the $\delta^{13}C$ signal. Denser C_3 vegetation (temperate forest) cover or soil development would lead to lower speleothem $\delta^{13}C$, while more open conditions or thin soils would shift $\delta^{13}C$ towards higher values (e.g. Scholz et al. 2012). A more open forest and/or thinner soil with reduced microbial activity and reduced production of soil CO_2 on the other hand would result in less negative $\delta^{13}C$ values (Genty et al. 2001, 2003).

Further information on soil and vegetation dynamics can be gained from the S/Ca signal (Fig. 6b). Generally, multiple sulfur sources have been identified, including sea spray, dust and volcanic aerosols as well as anthropogenic pollution (Frisia et al. 2005b, Wynn et al. 2010; Wolff et al., 2017). However, the observed long-term trend in S/Ca is most likely not caused by changes in volcanic aerosol loadings, which vary randomly. Similarly, changes in sea spray are unlikely to cause for the observed long-term trend because Bleßberg Cave is a continental site. Anthropogenic influence is similarly unlikely, as a major impact would be expected with industrialization, which is not covered by the youngest section of BB-1.

Inorganic and organic S is also derived from weathering and organic matter decomposition (Edwards 1998). Sulfur reduction and cycling also depends on redox potential Eh and pH conditions in the soil, although this is generally more significant in water-logged soils (Connell et al. 1968, Husson 2012). The Rendzina above Bleßberg Cave is characterized by high pH, low water holding capacity and strong ventilation. The predominant inorganic form of sulfur in aerobic soils is easy-leachable sulfate in the aqueous solution and attached to minerals. This also means that plant uptake of sulfate ions competes with direct leaching to the cave, with better developed soils resulting in improved retention and reduced S-loss through leaching. Sulfur can be retained in the soil by two main mechanisms, i.e. immobilization and adsorption, the relative importance of which can vary (Anderson 1988). The retention times of S can be long, depending on adsorptive capacity and the input of S (Edwards 1998). Importantly, increasing contact time between S and soil results in reduced SO^{2-}_4 leaching due to adsorption and/or transformation of S to less mobile components (Edwards 1998). The negative multi-millennial trend in S/Ca observed in BB-3, which is anticorrelated with Sr/Ca (Fig. 6b, c), suggests that increasing prior calcite precipitation (PCP) (as evidenced by higher Sr/Ca) results in enhanced S retention (lower S in speleothems), due to reduced infiltration and prolonged contact between S components and soil. The decrease of S in BB-3 through the early to mid-Holocene, thus, likely results from soil development, in tandem with diminishing (summertime) infiltration.

Interestingly, visual inspection of the S/Ca and Sr/Ca profiles reveals a positive correlation on multi-decadal to centennial timescales independent from the long-term trend (Fig. 4), indicating that other factors partake in forcing sulfur mobility on these timescales. Changes in weathering rates, aerosol input or soil activity are all potential candidates for this high-frequency variability. Still, the responsible mechanism must affect both S/Ca and Sr/Ca to cause the observed pattern. Enhanced S immobilization and mineralization and low PCP under colder and wetter conditions, reflected in lower S and Sr content in the stalagmites (Edwards 1998) is a viable explanation. In summary, both proxies are interpreted as indicators of local conditions, which of course are embedded and moderated by the larger-scale climatic milieu.

The climate in the study region shows no clear seasonality in precipitation (Fig. 2b), but evapotranspiration, and thus effective infiltration, varies throughout the year, with a maximum during the winter months (Fig. 2d). Infiltration-sensitive proxies should therefore be able to record infiltration changes, with a bias towards the warm season and reduction in spring to autumn infiltration. Dry conditions can lead to (more) open conditions in soil and epikarst, and associated CO_2-degassing from infiltrating water into epikarst air pockets and the cave atmosphere, which in turn allows PCP (Fairchild & McMillan 2007, Breitenbach et al. 2015). PCP can alter the elemental composition of dripwater feeding the stalagmites and increases the Sr concentration in the aqueous solution (Fairchild & Treble 2009).

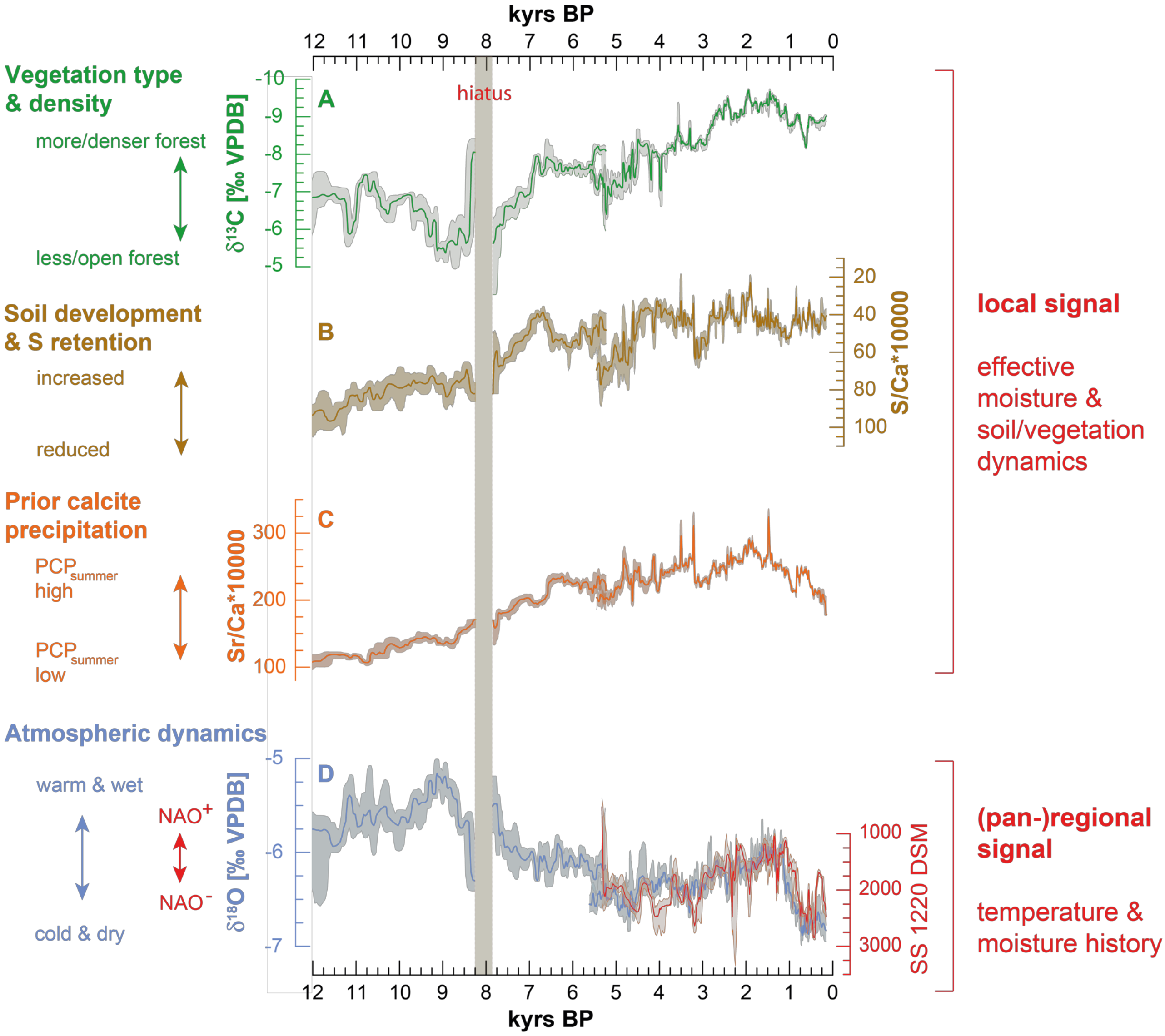

Figure 6: Bleßberg Cave proxy records and their interpretation. A) δ¹³C values from BB-1 and BB-3 indicate changes in vegetation density. B) S/Ca records from BB-1 and BB-3 reflect soil development and sulfur retention. C) Sr/Ca shows long-term but opposite trends to S/Ca. D) δ¹⁸O values from both stalagmites, with lower values being observed during cold and dry periods, stronger Siberian High influence on the study site. Lower δ¹⁸O values (blue) are frequently observed during intervals of negative NAO (higher DSM values in lake SS1220, red curve). The DSM record is based on the updated age-depth model provided in this study.

The Sr/Ca profile across both stalagmites shows a positive trend throughout the early to mid-Holocene (11 ka BP to 6 ka BP, Fig. 6c). This trend is interpreted as resulting from increasing summertime PCP with increasing insolation and a more negative moisture balance in summer (Kalis et al. 2003, Russo & Cubasch 2016). Subsequent to the Holocene Thermal Maximum (Wanner et al. 2011), Sr/Ca ratios remain on a relatively constant level (even if the offset between both stalagmites is taken into account). The observed higher centennial-scale variability after ca. 5.5 ka BP is likely due to the fact that this stalagmite received fracture flow with a faster response to surface conditions. Several positive Sr peaks at 3.5 ka, 3.2 ka and 1.5 ka BP suggest intense, but short-lived periods of moisture reduction and intensified PCP. Since about 2 ka BP, Sr/Ca values decrease again, possibly related to weakening summer insolation (Russo & Cubasch 2016) and improved hydroclimatic conditions with higher effective infiltration. Strong PCP also results in increased degassing of CO_2 and precipitation of calcite (Fairchild & McMillan 2007) and can, thus, also be reflected in less negative $\delta^{13}C$ values. However, as outlined above, the $\delta^{13}C$ signal is largely unrelated to Sr and governed by vegetation dynamics.

5.1.2 Controls on $\delta^{18}O$ in precipitation and dripwater

5.1.2.1 Regional factors controlling $\delta^{18}O$ in precipitation

Precipitation is delivered to Bleßberg Cave throughout the year and mainly from the North Atlantic, without clear seasonal maximum (Fig. 2) but higher effective infiltration in the winter season (Fig. 3). The oxygen isotopic composition in precipitation ($\delta^{18}O_p$) is strongly linked to air temperature and the NAO conditions (Baldini et al. 2008). These relationships are exemplified with $\delta^{18}O$ data from meteorological stations Hof, Leipzig and Wasserkuppe/Rhön in Fig. 3a; at all three stations $\delta^{18}O_p$ is highest in summer, with a total annual amplitude of ca. 4 to 5‰. Thus, under higher temperatures and/or a positive NAO, $\delta^{18}O_p$ is expected to increase. The temperature control on $\delta^{18}O_p$ in the region (using Hof, Leipzig and Wasserkuppe/Rhön as reference) is ca. +0.23‰°C^{-1}, thus counter-balancing the negative temperature effect on carbonate precipitation. This is different to Bunker Cave, for which Wackerbarth and coworkers (2010) observed an additional effect of the amount of winter precipitation on precipitation $\delta^{18}O$, which we do not observe for the reference stations used here.

5.1.2.2 Local factors controlling $\delta^{18}O$ in infiltrating water

Local factors that influence $\delta^{18}O$ in soil, epikarst and cave include i) evaporation of soil water, ii) evaporation of dripwater, iii) CO_2-degassing of dripwater in the cave, iv) temperature, and v) mixing of older and younger water in the epikarst. Evaporation of soil water is more pronounced in the summer season (Fig. 2), but is unlikely to contribute to changes in Bleßberg Cave dripwater on short time scales because May and August samples are not significantly enriched relative to winter month samples (Fig. 3a) and because no secondary evaporation trend, with values following a slope lower than 8, is observed (Fig. 3b). Evaporation of dripwater can be excluded based on the same observations and the fact that in cave relative humidity is stable >98 %. CO_2 degassing from dripwater into the cave air during times of lower drip rates might affect $\delta^{18}O$ (Mühlinghaus et al. 2009). However, this effect is very small (i.e. $\Delta\delta^{18}O$ ~0.1‰/1000 sec. at T=10°C, Deininger et al. 2012) and would not explain $\delta^{18}O$ changes in the range of 0.5 to 2 permil over multi-decadal to centennial time scales. Temperature effects on the dripwater are unlikely because the cave air temperature does not vary appreciably ($T_{cave\ air}$ = 8.7±0.1°C). Finally, mixing of infiltration waters of different age is likely the main reason for the relatively stable dripwater $\delta^{18}O$ (Fig. 3a) and a very narrow range along the GMWL (Fig. 3b). The small offset between the two individual stalagmites, and the dampened variability found in BB-3 are evidence for mixing of waters in the epikarst, which differ for the two stalagmite sites.

5.1.2.3 $\delta^{18}O$ as proxy of atmospheric circulation

The Bleßberg Cave $\delta^{18}O$ ($\delta^{18}O_{spel}$) record (Fig. 6d) integrates precipitation history and the corresponding $\delta^{18}O$ signal in precipitation ($\delta^{18}O_p$), seasonal changes in infiltration, and temperature in a complex fashion and thus records longer-term pan-regional environmental dynamics. Given the observed seasonal infiltration pattern (Fig. 2), it can be argued that both dripwater and speleothem $\delta^{18}O$ values represent a mean signal that is slightly biased towards the winter season. This is similar to other German caves (e.g. Mischel et al. 2015, Wackerbarth et al. 2010). Thermal conditions in the cave are stable and cave air temperature changes over the course of the Holocene are unlikely to have caused the observed 2‰ amplitude in $\delta^{18}O_{spel}$ values. Assuming a (cave) temperature dependence of the isotopic composition during carbonate precipitation of ca. −0.24‰°C^{-1} (McDermott 2004), counter-balanced by a positive $\delta^{18}O_p$/T relation of ca. +0.23‰°C^{-1} would imply $\Delta T_{Holocene}$ ~8°C to explain the observed 2‰, which seems unrealistically high for the last 9-10 ka BP. Several lines of evidence suggest an important influence of atmospheric circulation, moisture source dynamics and $\delta^{18}O_p$ on $\delta^{18}O_{spel}$ in Bleßberg Cave. A significant positive correlation has been found between the NAO and $\delta^{18}O_p$ over Central Europe (Hurrell 1995, McDermott et al. 2011, Baldini et al. 2008, Comas-Bru et al. 2016). The strong positive impact of the winter NAO on $\delta^{18}O_p$ is caused by more frequent inflow of cold, isotopically depleted precipitation during negative NAO phases (Baldini et al. 2008). A tentative link between NAO and Bleßberg $\delta^{18}O_{spel}$ is found in the visual similarity between BB-1 $\delta^{18}O$ and the updated detrital silicate mineral (DSM) record from lake SS1220 ($DSM_{SS1220} = \Sigma_{[Sr,\ Zn,\ Ti]}$, Olsen et al. 2012, Fig. 6d). For this study we updated the SS1220 chronology by using the Intcal13 calibration curve (Reimer et al. 2013) to re-calibrate the ^{14}C measurements originally reported in Olsen et al. (2012). We then sampled 5,000 stratigraphically ordered age models from the multimodal re-calibrated ages, which resulted in a 5,000 member DSM_{SS1220} proxy record ensemble. Warmer conditions with increased meridional flow of warm maritime air over SW Greenland are normally associated with negative NAO, while positive NAO conditions are characterized by cold, dry air masses over southern Greenland (Olsen et al. 2012). In Central Europe, negative (positive) NAO conditions are linked to colder (warmer) and drier (wetter) air under increased (decreased) Siberian High influence, reflected in more negative (positive) $\delta^{18}O_p$ and $\delta^{18}O_{spel}$ values (Baldini et al. 2008).

Thus, climatic conditions in Central Europe are not solely determined by maritime (NAO) influence from the Atlantic, but also by the SH. The winterly SH is another major player that influences atmospheric circulation, precipitation, and temperature (Berry & Chorley 2010, Tubi & Dayan 2012). The interaction between the NAO and the SH results from complex tropospheric and stratospheric linkages (Cohen et al. 2001, Cohen et al. 2014; Ambaum & Hoskins 2002). Both systems are intimately linked with the Arctic Oscillation (AO), which has been suggested to lag NAO dynamics by a few days (Ambaum & Hoskins 2002). A positive NAO leads to a stronger stratospheric vortex and a deepened low pressure cell over the North Pole, and effectively a positive AO. This in turn results in stronger Westerlies and fewer and smaller meanders of the zonal jet stream (Cohen et al. 2014). Under such conditions, the strong Westerlies transport more and warmer moisture from the N Atlantic towards Europe and into Eurasia and the SH has rarely the chance to reach Central Europe. In a negative NAO/AO mode on the other hand the Arctic low pressure system is weaker and the zonal jet is characterized by increased meandering which allows frequent atmospheric blocking and intrusion of cold air from the north/northeast. The Westerlies are weaker and frequently redirected southward, thus delivering less moisture to Germany, while the intruding Arctic air is very cold. Thus, the influence of the SH increases under negative NAO/AO conditions. Inflow of north-easterly continental air under strong SH conditions replaces warm maritime air from the west. The increasing SH influence with distance from the Atlantic coast is directly expressed in the change from a maritime Cfb climate to a continental Dfb climate at ca. 10°E (Peel et al. 2007). Thus, $\delta^{18}O_{spel}$ from Bleßberg Cave is sensitive to shifts of the boundary between the two climate zones.

5.2 Local and pan-regional environmental changes in Central Europe

The multi-proxy datasets from BB-1 and BB-3 allow detailed insights into both local and pan-regional environmental conditions throughout the Holocene. Below, we first discuss how the local environment evolved after the last deglaciation. Then, we compare the climatic conditions in Thuringia to those in Europe and the North Atlantic realm and discuss the role of a shifting Cfb-Dfb climate boundary and jet stream as explanation for the differences between sites.

5.2.1 Local environmental changes

We use the $\delta^{13}C$, S/Ca, and Sr/Ca time series to reconstruct local vegetation, soil and infiltration dynamics through the Holocene. High $\delta^{13}C$ values between the Late Glacial and the onset of the Holocene (Fig. 6a) point to an open, and possibly grassland vegetation, typical for periglacial conditions (Hahne 1991, Bebermeier et al. 2018). After a short-lived excursion to drier and/or colder conditions shortly before 11 ka BP, the $\delta^{13}C$ record trended towards higher values for the next ca. 2400 years, potentially indicative of an early coniferous forest (Hahne 1991; Bebermeier et al. 2018). Decreasing S/Ca and low, slowly increasing Sr/Ca values between 11 and 9 ka BP indicate cumulative soil development and improved sulfur retention with sufficient effective infiltration to minimize summerly PCP (Figs. 6b, c). The Preboreal to early Holocene development is comparable to that in the southern Harz Mountains, ca. 100 km to the north of our study site (Bebermeier et al. 2018).

Elevated $\delta^{13}C$ values after ca. 9 ka BP (the onset of the Boreal, *sensu* Hahne 1991) point to a return to a more open forest, or a change in vegetation composition. Pollen profiles from the Rhön (Hahne 1991), ca. 40 km west of Bleßberg Cave, and Eichsfeld (Bebermeier et al. 2018) suggest replacement of pine forest by *Corylus* communities which prefer warmer conditions. A change to more open forest is not mirrored in the S/Ca and Sr/Ca ratios, suggesting that it was not accompanied by increased (summer) drought and related soil or infiltration changes. Less negative $\delta^{18}O$ values at ca. 9 ka BP also suggest relatively warm/wet conditions (Fig. 6d). A drastic decrease in both $\delta^{13}C$ and $\delta^{18}O$ between ca. 8.7 ka BP and 8.4 ka BP, concurrent with a slight increase in Sr/Ca might be explained by a post-glacial afforestation under drier summer conditions and intensified PCP. A scenario where the vegetation composition changed from deciduous to coniferous forest is less likely because one would expect a shift to more positive $\delta^{13}C$ values (Amiotte-suchet et al. 2007), opposite to the observed trend. A concurrent trend towards more negative $\delta^{18}O$ values suggests cooling and drying and/or increased winter precipitation prior to the 8.2 ka event.

The hiatus found in BB-3 covers ca. 400 years, starting 8.26 and ending 7.85 ka BP, with a minimum and maximum length of 64 and 710 years, respectively, when considering the chronological uncertainties in the BB-3 record. The hiatus corresponds closely with the 8.2 ka event (Mayewski et al. 2004, McDermott 2004) and can only be explained by complete absence of dripwater, caused either by flooding or infilling of the cave passage, re-routing of the water, prolonged drought, or permafrost conditions (Vaks et al. 2010, 2013; Lechleitner et al. 2017). A return of permafrost during the 8.2 ka event seems the most likely scenario because we have no evidence in support of infilling of the cave with sediment or water, or drought with zero effective infiltration, which should be reflected in increased Sr/Ca (increased PCP). The development of permafrost (i.e. at least two consecutive years with ground temperature <0°C, Harris et al. 2009) during the 8.2 ka event would require a decrease in mean annual air temperature of >6°C with respect to modern conditions, which at first glance seems very high. A drastic, although not reaching 6°C, decrease in temperature during the 8.2 ka event has been found in western and northern Europe (Seppä et al. 2009, Vincent et al. 2011). However, given the complex interaction between geomorphology, geology, precipitation, air and ground temperatures (Harris et al. 2009) local permafrost development in hilly Thuringia seems plausible. More detailed work is needed to reconstruct the climatic conditions surrounding the 8.2 ka event.

After ca. 7.8 ka BP, conditions improved and stalagmite growth commenced again, with rapid soil development and denser forest vegetation, as seen in lower S/Ca ratios and $\delta^{13}C$ values. This climatic amelioration was accompanied by slightly increased PCP, likely due to warmer summers (Fig. 6c). After ca. 6.7 ka BP, soil development and/or sulfur retention level out, with only two excursions around 5.5 and 3 ka BP, when conditions seem to have been comparatively drier. Vegetation, however, was likely more dynamic, as reflected in noticeable variations in $\delta^{13}C$ between

5.5 and 3.5 ka BP (Fig. 6a), sometimes together with increased PCP. A trend to more negative $\delta^{13}C$ values after 3 ka BP suggests increased forest cover, which was reversed only in the last ca. 1500 years, possibly related to deforestation activities of Bronze Age settlers (Bebermeier et al. 2018).

5.2.2 Pan-regional climatic changes

Today, Central Europe is governed by maritime Cfb climate, while eastern Europe is characterized by continental Dfb climate (Kottek et al. 2006, Peel et al. 2007). The meteorological border between these two climatic provinces is located over Germany (Fig. 1) and has also been identified as a significant shift in the orientation of precipitation isochron pattern (Rheinwalt et al. 2016). Importantly, over time this climatic boundary is not stationary and shifts, depending on climatic conditions (Kottek et al. 2006). It should, in principle, be possible to detect past changes of the geographical position of this climatic divide if sufficient well dated and resolved proxy time series were available from locations distributed across Europe. Links between reconstructions that are located on each side of the boundary and influenced by factors that govern climate in the respective zone can give insights how this boundary shifted in space and time. Using only one additional record from the opposing climate zone would not suffice however, because one would find either positive, negative or zero correlation. While the latter two scenarios could be interpreted to indicate a climate boundary between the two sites, the first scenario could only suggest a common forcing factor, but would not clarify whether the climate boundary is located east or west of both sites. Thus, at least one third record is needed to identify the position of the boundary relative to the sites, and the controls relevant at each location.

To estimate the geographical position of the Cfb-Dfb boundary, we use two time series from the North Atlantic realm in addition to the Bleßberg Cave BB-1 record (see Figs. 1 and 7). The first of these records is the $\delta^{18}O$ time series from stalagmite BU-4 ($\delta^{18}O_{BU4}$) from Bunker Cave in western Germany (Fohlmeister et al. 2012). The $\delta^{18}O_{BU4}$ record has been interpreted as reflecting a complex signal of temperature and moisture supply. While the $\delta^{18}O$ signal in Bunker Cave reflects multiple processes, less negative $\delta^{18}O$ values indicate colder and/or drier conditions, while lower values suggest warmer and/or wetter climate. Multi-annual variations in surface temperature and precipitation amount have been linked to NAO dynamics (Wackerbarth et al. 2010, Riechelmann et al. 2017).

The second reconstruction used to test the concept of a shifting climate boundary is a multi-element proxy record of DSM input from lake SS1220 (DSM_{SS1220}) in southwestern Greenland (Olsen et al. 2012). The DSM record is the sum of Sr, Zn and Ti counts observed in the lake sediment profile, in a similar fashion as proposed by Saarni et al. (2016), and is used here to infer NAO conditions. Higher DSM values indicate increased sediment transport associated with snowmelt and runoff into the lake. In southwestern Greenland increased runoff and sediment supply are expected in mild and/or short winters with longer thaw periods and prolonged runoff; conditions that have been associated with negative NAO phases (Olsen et al. 2012). High DSM values are thus interpreted as representative for negative NAO phases (see Fig. 6d).

These time series and the Bleßberg $\delta^{18}O$ record from BB-1 ($\delta^{18}O_{BB1}$) reflect relevant circulation features with sufficient resolution and chronological control for the last ca. 4,000 years to allow a first estimation of past boundary dynamics. To establish the Cfb-Dfb boundary, we estimate correlations between the three records, which we then link with the information on the atmospheric circulation patterns (NAO index and SH strength) assigned to the proxy records to estimate the position of the climate boundary. It must be kept in mind that the interpretation of $\delta^{18}O$ from Bleßberg and Bunker caves is opposite in sign, with lower $\delta^{18}O$ values in Bleßberg Cave indicating colder and drier conditions under a more pronounced SH and negative NAO influence, while reflecting wetter and warmer (maritime) conditions above Bunker Cave. This relationship could change however due to changes in seasonal precipitation pattern and resulting slopes of the $\delta^{18}O_p$-T relationship. The obtained correlation patterns allow the identification of the following Cfb-Dfb boundary position scenarios (Fig. 7):

- **Scenario 1 Cfb-Dfb boundary east of Bleßberg Cave**

The first scenario is similar to modern conditions (Kottek et al. 2006), but with the Cfb-Dfb boundary located shifted further east of Bleßberg Cave. The maritime influence reaches towards eastern Central Europe while the Siberian High influence on western Europe is relatively weak. Under such conditions, Bleßberg and Bunker caves would record the same maritime climate and a common forcing with strongly positive NAO influence. The interpretation of $\delta^{18}O_{BB1}$ would be reversed, because continentality, and with it the slope of the $\delta^{18}O_p$-T relationship would be lowered (Bowen 2008). Consequently, Bleßberg Cave would react much like Bunker Cave, with a positive correlation between the two $\delta^{18}O$ records, while DSM_{SS1220} values should be lowered (Fig. 7). A boundary east of Bleßberg Cave thus would result in a positive correlation between all three records. Modern observational data show a stronger Atlantic influence on Central Europe and a significant positive link between NAO index and precipitation $\delta^{18}O$ at Wasserkuppe/Rhön near Bleßberg Cave (Baldini et al. 2008). Such conditions occur when the zonal jet is stronger and less meandering (Cohen et al. 2014). Unfortunately, since the Bleßberg Cave record does not cover the last few hundred years, we cannot test the inferred links with meteorological records.

- **Scenario 2 Cfb-Dfb boundary between Bleßberg Cave and Bunker Cave**

A second scenario would see the Cfb-Dfb boundary located between the two German caves, with Bunker Cave being governed by maritime climate and Bleßberg Cave by continental climate conditions. Under these conditions, $\delta^{18}O_{BB1}$ should decrease (due to increased continentality and resultant colder winters), while the $\delta^{18}O_{BU4}$ and DSM_{SS1220} records might remain unchanged or increase compared to scenario 1, with the cave records reflecting atmospheric dynamics related to the climatic regime on either side of the Cfb-Dfb boundary. As a result, negative correlation between $\delta^{18}O_{BB1}$ and $\delta^{18}O_{BU4}$ should be found, while the Greenland DSM_{SS1220} record would be expected to show negative to nil correlation to $\delta^{18}O_{BB1}$, but remain positively linked to $\delta^{18}O_{BU4}$, as long as the Westerlies exert some influence on Bunker Cave (Fig. 7). Scenario 2 would be characterized by frequent SH influence on Central Europe, a consistently changing NAO and stronger meandering of the jet stream, but relatively mild conditions.

- **Scenario 3 Cfb-Dfb boundary east of Bleßberg Cave**

A third scenario might occur where the climate boundary is positioned east of Bleßberg Cave, similar to scenario 1, but with more stable climate conditions. In scenario 3, both speleothem $\delta^{18}O$ records would be expected to be influenced by maritime climate, with rare incursions of cold Arctic air during winter and strongly positive NAO (Fig. 7b). The interpretation of $\delta^{18}O_{BB1}$ would be reversed (as in scenario 1), because of strongly diminished continentality. Bleßberg and Bunker cave would be more responsive to oceanic conditions, reflected in a positive correlation between both $\delta^{18}O$ records. A negative correlation between $\delta^{18}O_{spel}$ and DSM_{SS1220} would result, with lower $\delta^{18}O_{spel}$ and increased DSM values reflecting negative NAO dynamics and *vice versa*.
This scenario differs from scenario 1 in that it includes a poleward displacement of the jet stream in a generally warmer atmosphere (Archer and Caldeira 2008, Woolings and Blackburn 2012), so that the maximum moisture transport would be redirected towards Scandinavia. Concurrently, the Siberian High influence on Central Europe would be diminished, which in turn would lead to more stable conditions, albeit with decreased winter moisture and higher PCP at Bleßberg Cave (Fig. 6). An intensified and poleward jet and positive NAO result from a large pressure difference between a cold Arctic and very warm mid-latitudes (Archer and Caldeira 2008). This interpretation would explain higher $\delta^{18}O_{BB1}$ values (Fig. 7b) as response to drier winter conditions in Thuringia, and lower $\delta^{18}O_{BU4}$ values, due to warmer and/or wetter conditions at Bunker Cave. Higher winter precipitation would be expected in Northern Europe.

- **Scenario 4 Cfb-Dfb boundary between both caves**

A fourth scenario has been found in the correlation analyses whereby the $\delta^{18}O_{BU4}$ time series shows an increasing trend, while the $\delta^{18}O_{BB1}$ record shows an opposite trend (and *vice versa*), i.e. both cave records are anticorrelated. The DSM record is positively correlated with the $\delta^{18}O_{BB1}$ time series. The $\delta^{18}O_{BB1}$ values are slightly more negative compared to scenario 1 (Fig. 7b) while the $\delta^{18}O_{BB1}$ and DSM_{SS1220} values are higher. These observations suggest a moderate to strong influence of the Siberian High on Bleßberg Cave and a pronounced negative NAO. The lower $\delta^{18}O_{BB1}$ values and the positive correlation of $\delta^{18}O_{BB1}$ with DSM_{SS1220} suggest winter conditions with frequent SH influence on Bleßberg Cave and negative NAO (i.e. cold winters bringing ^{18}O-depleted precipitation *sensu* Baldini et al. 2008). We hypothesize that the climatic boundary is located between both caves.

- hypothetical **Scenario 5 Cfb-Dfb boundary west of Bunker Cave**

Theoretically, a fifth scenario could occur if very cold conditions would lead to a westward retreat of the Cfb-Dfb boundary. Such conditions might have prevailed in periods with southward displaced jet stream, e.g. the late glacial before northern hemisphere warming would allow the maritime climate to reach Central Europe. This scenario is not observed in the discussed late Holocene records. At Bunker Cave increased continentality would result in a positive slope of the $\delta^{18}O_p$-T relationship and a reversed interpretation of $\delta^{18}O_{BU4}$ (higher $\delta^{18}O_{BU4}$ indicating warmer conditions). Since continental conditions would prevail, a positive correlation between the two cave records is expected. If the jet stream would be located far west of Bunker Cave, the latter would loose sensitivity to the maritime climate. This would be reflected in a reduced or lacking correlation (in either direction) between the cave proxies and the DSM_{SS1220} record, which would be expected to still be governed by North Atlantic climate variability and indicative of the NAO state. Western Europe would be expected to be more frequently affected by the winterly Siberian High.

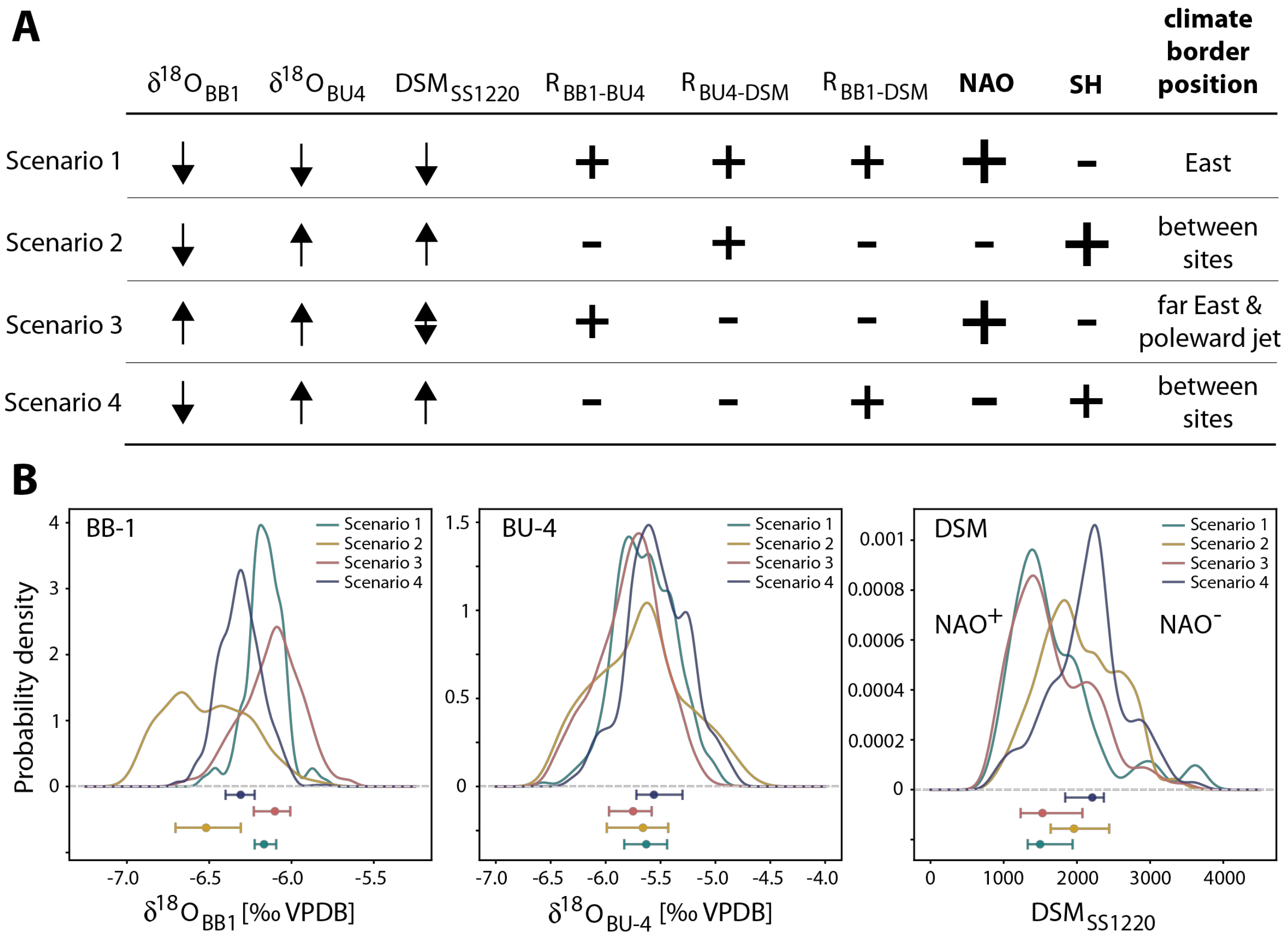

Figure 7: A) Interpretation of proxy records, their correlations (R), and inferred state of the North Atlantic Oscillation and the Siberian High in the four scenarios of the position of the Cfb-Dfb boundary over Europe. The size of the signs indicates the relative strength of the parameter (i.e. the correlations are weaker). **B)** Probability densities for the three records for each of the four observed scenarios.

The correlations between the three sites Bleßberg Cave, Bunker Cave and Greenland lake SS1220 (Fig. 8d-f) allow us to estimate changes in the longitudinal position of the Cfb-Dfb boundary and the jet stream over the last ca. 4,000 years. NAO and SH pattern are inferred from the DSM_{SS1220} profile and the $\delta^{18}O_{BB1}$ time series, respectively. The correlations, the NAO index, relative strength of the Siberian High, and the inferred position of the climate boundary are summarized in Fig. 8g.

Prior to about 3.9 ka BP, concurrent positive correlation between $\delta^{18}O_{BB1}$ and $\delta^{18}O_{BU4}$ and negative correlation between the cave records and DSM_{SS1220}, suggest that the Cfb-Dfb boundary was located east of Bleßberg Cave (scenario 3) and that Central Europe was under influence of maritime climate, likely with a moderate winterly SH influence at Bleßberg Cave. With a climate boundary shifted east the influence of the NAO on Central Europe was likely increased. Relatively high DSM values suggest negative NAO conditions, which would go in hand with stronger meandering of the zonal jet and cold air inflow during winter.

After 3.9 ka BP we find a reversed $\delta^{18}O_{BB1}$ and $\delta^{18}O_{BU4}$ correlation (scenario 4), which we tentatively interpret as a ca. 200-year long transition phase from scenario 3 to scenario 2. Insufficient data points in the DSM_{SS1220} record prevent computing the correlations with $\delta^{18}O_{BB1}$ and $\delta^{18}O_{BU4}$ between 3.7 and 3.3 ka BP (Fig. 8e, f) and statements regarding the NAO impact on European climate must remain vague. Intermediate DSM values suggests variable NAO conditions. The negative correlation between $\delta^{18}O_{BB1}$ and $\delta^{18}O_{BU4}$ can be used however to infer a likely position for the Cfb-Dfb boundary between the two caves (scenario 2). This interval was followed by a shift back to scenario 4. This period with a negative NAO and strong SH lasted for only about a century (~3.3-3.2 ka BP) and was then succeeded by a 500-year long period of the similar scenario 2, with negative correlations between $\delta^{18}O_{BB1}$ and $\delta^{18}O_{BU4}$ and $\delta^{18}O_{BB1}$ and DSM_{SS1220}. At this time the Cfb-Dfb boundary was located between the two caves; both the SH and the NAO exerted their influence on their respective climate zones. A strong SH at that time has also been identified by Mayewski et al. (2004) in the GISP2 ice core potassium record and frequent negative NAO conditions have been noted between ca. 3.1 ka and 2.5 ka BP by Olsen et al. (2012).

Around 2.7 ka BP another transition occurred, found as a ca. 300-year interval with unclear but likely eastward boundary shift. Considering the available evidence, it is likely that this time was characterized by higher climate variability, with continued boundary shifts and variable SH and NAO strength. The low DSM_{SS1220} values suggest that the NAO shifted to a positive phase at the time. At 2.4 ka BP a prominent, 500-year long interval of near-modern climate set in, with the Cfb-Dfb boundary located between both caves. The SH had influenced winter conditions concurrent with a positive NAO, as indicated by the DSM values.

This maritime interplay was rapidly (within ca. 100 years) replaced by a more maritime climate that lasted from ~1.9 ka BP to ~1.1 ka BP (scenario 3). This period was characterized by a concurrent poleward displacement of the jet stream and more stable conditions in Central Europe. Winters at

Bleßberg Cave were most likely drier due to this northward shift of the Westerlies which would bring increased winterly moisture to Scandinavia and Bunker Cave, while the Thuringian summers were seemingly warm and dry (as indicated by increased PCP, Fig. 6). The DSM_{SS1220} record suggests a positive NAO. Saarni et al. (2016) noted increased snow accumulation during positive NAO, consistent with our interpretation.

A last change is recorded in our time series at around 1.1 ka BP, when the climate boundary shifted westward, to remain between the two caves until at least 500 years ago when our Bleßberg record ends. This last period was characterized by a strong SH and concurrently variable and frequently negative NAO, which together left winterly Germany colder. The inferred strong SH is supported by the GISP2 K record (Mayewski et al. 2004). The inferred negative NAO at the time (covering the Medieval Climate Anomaly) is also supported by a tree ring-based reconstructions of a multi-centennial mega-drought in Scandinavia (Helama et al. 2009) and humid and mild summers in Central Europe (Büntgen et al. 2011).

Above Bleßberg Cave summertime PCP diminished slowly, indicating increasing summer infiltration. In western Germany (at Bunker Cave) higher climate variability can be inferred from the $\delta^{18}O$ record (Fig. 8b), which can be understood if we assume less severe influence of the SH on local conditions at its far western limit.

Because the last 500 years are not covered by the Bleßberg stalagmite, we cannot connect our reconstruction with historical and meteorological data. The Cfb-Dfb climate boundary continued to migrate eastward, is currently located near the eastern border of Poland, and expected to shift even further east under global warming conditions (Kottek et al. 2006).

In summary, the comparison of multiple sites allows the identification of shifts in the mean position of the Cfb-Dfb climate boundary over the last ca. 4,000 years, depending on the relative strength and dynamics of the Siberian High and the Westerlies and the position of the jet stream. To refine this reconstruction, a denser network of records would be required, possibly by exploiting the new Speleothem Isotope Synthesis and Analysis database (Atsawawaranunt et al. 2018). With improved spatio-temporal coverage it might also be possible to deduce directionality of forcings and determination of the speed of such climate transitions.

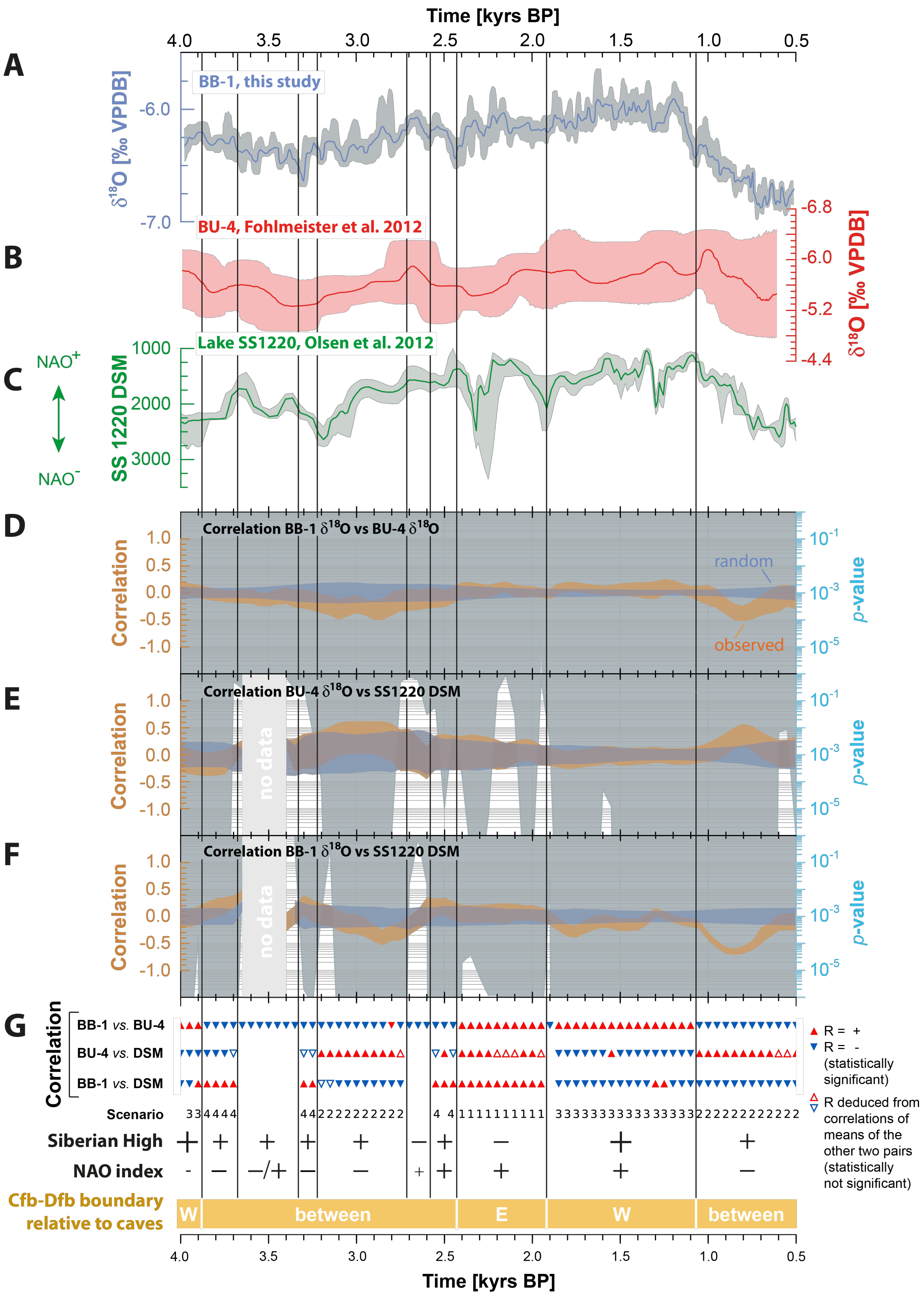

Figure 8: Proxy records from Bleßberg ($\delta^{18}O_{BB1}$, A), Bunker Cave ($\delta^{18}O_{BU4}$, B), and Greenland (DSM_{SS1220}, C) covering the last 4,000 years are correlated to highlight non-stationary relationships. Solid lines in A-C denote the

median proxy value and shades represent the inter-quartile ranges as obtained from COPRA proxy record ensembles composed of 5,000 age-depth simulations each. The DSM_{SS1220} profile is based on an updated chronology in which the IntCal13 calibration curve was used to calibrate the radiocarbon ages. Randomly chosen pairs proxy records from the COPRA ensembles are used to estimated the correlations (orange bands, D-F) between each pair of records using the NESTool methodology that allows estimation of correlation for irregularly sampled time series. The relationship between the records is compared to that obtained from an ensemble of pairs of randomized time series (blue bands), and this is quantified with the *p*-value of a 2-sample Kolmogorov-Smirnov test (light blue shaded backgrounds, see section 4.5 for details). (G) Correlation summary and inferred Siberian High strength and NAO index, as well as estimates of the position of the Cfb-Dfb climate boundary. Solid triangles indicate statistically significant correlations, while empty triangles refer to statistically not significant values that are deduced from the (significant) correlations between the median values of the other pairs. Insufficient data points in the DSM_{SS1220} record prevent computing the correlations with $\delta^{18}O_{BB1}$ and $\delta^{18}O_{BU4}$ between 3.7 and 3.3 ka BP.

6. Conclusions

Two U-series dated stalagmites (BB-1 and BB-3) from Bleßberg Cave, Thuringia, are used to reconstruct local and (pan-)regional environmental conditions. The time series from stalagmites BB-1 and BB-3 cover the entire Holocene with the exception of a ca. 400-year long hiatus at 8.2 ka. All proxies discussed above respond to local processes, which themselves are governed by regional atmospheric dynamics. In this way, they all inform on individual aspects of environmental conditions active at the time of speleothem deposition. $\delta^{13}C$, S/Ca and Sr/Ca inform us about local environmental changes, including vegetation and soil changes above the cave, as well as prior calcite precipitation linked to effective infiltration through the course of the Holocene. Stalagmite $\delta^{18}O$ is interpreted as recorder of changes in moisture source dynamics and temperature and thus as (pan-)regional signal. We combine the Bleßberg Cave $\delta^{18}O$ record with distal proxy reconstructions to infer changes in the relative importance of marine and continental conditions on Central European environment.

For the last ca. 4,000 years we compared the BB-1 $\delta^{18}O$ record with the $\delta^{18}O$ profile from stalagmite BU-4 from Bunker Cave in western Germany and a detrital silicate material record from lake SS1220 (SW Greenland) and estimate the changes in the Cfb-Dfb climate boundary, as well as the strength of the Siberian High and dynamics of the North Atlantic Oscillation. We find a complex temporal pattern with repeated multi-centennial scale E-W shifts of the Cfb-Dfb boundary. The local environment at Bleßberg Cave reacts to an intensified Siberian High mainly with reduced soil development and increased prior calcite precipitation during the warm season, due to reduced winterly precipitation.

The interpretative value of the presented estimate of the dynamics of the climate boundary is currently limited by the low number of well-dated and highly resolved reconstructions from Europe. Using this approach to integrate available datasets from additional archives, including speleothem, tree-ring and pollen data, will help refine and possibly quantify our insights in Holocene climate and vegetation dynamics. We are confident that with improved spatial coverage the history of climate boundaries will become recognizable at much finer scale. Discrepancies between spatially distributed reconstructions might indicate competing environmental forcings and can be exploited to resolve climatic regimes in different climate zones.

Acknowledgements

We thank Brigitte Richert (GFZ Potsdam) for μXRF analysis, and Rudolph Naumann (GFZ Potsdam) for support with XRD and XRF analyses, Heike Rothe (GFZ Potsdam) for ICP-MS analysis and Michael Gömmel for sample preparation. Andreas Hendrich (GFZ Potsdam) helped preparing figure 1. Frank Haubrich, Saxony, helped with detailed information on soil composition. The VdHK e.V. kindly supports this study with monitoring equipment and the Thüringer Höhlenverein, Erfurt, is thanked for logistical support. This study received funding from the European Union's Horizon 2020 Research and Innovation programme under the Marie Skłodowska-Curie grant agreement No 691037. Denis Scholz acknowledges funding by the German Research Foundation (DFG) through grants SCHO 1274/9-1 and SCHO 1274/10-1; Norbert Marwan and Bedartha Goswami acknowledge funding by DFG MA MA4759/8-1.

Data availability

The datasets presented here will be available on the website of the corresponding author (SFMB) and on public repository, including https://www.pangaea.de. Data can also be requested by contacting SFMB directly.

References

Anderson D.W. (1988) The effect of parent material and soil development on nutrient cycling in temperate ecosystems. Biogeochemistry 5, 71–79, doi: 10.1007/BF02180318.

Ambaum M.H.P. and Hoskins B.J. (2002) The NAO Troposphere–Stratosphere Connection. Journal of Climate 15, 1969-1978, doi: 10.1175/1520-0442(2001)014<3495:AOONAO>2.0.CO;2.

Amiotte-suchet P., Linglois N., Leveque J., Andreux F. (2007) ^{13}C composition of dissolved organic carbon in upland forested catchments of the Morvan Mountains (France): Influence of coniferous and deciduous vegetation. Journal of Hydrology 335, 354–363, doi: 10.1016/j.jhydrol.2006.12.002.

Archer C.L. and Caldeira K. (2008) Historical trends in the jet streams. Geophysical Research Letters 35, L08803, doi:10.1029/2008GL033614.

Atsawawanunt K., Comas-Bru L., Mozhdehi S.A., Deininger M., Harrison S.P., Baker A., Boyd M., Kaushal N., Ahmed S.M., Arienzo M., Brahim Y.A., Bajo P., Braun K., Burstyn Y., Chawchai S., Duan W., Hatvani I.G., Hu J., Kern Z., Labuhn I., Lachniet M., Lechleitner F.A., Lorrey A., Pérez-Mejías C., Pickering R., Scroxton N. and SISAL Working Group Members (2018) The SISAL database: a global resource to document oxygen and carbon isotope records from speleothems. Earth Systems Science Data 10, 1687-1713, doi: 10.5194/essd-2018-17.

Baldini L.M., McDermott F., Foley A.M., Baldini J.U.L. (2008) Spatial variability in the European winter precipitation δ^{18}O-NAO relationship: Implications for reconstructing NAO-mode climate variability in the Holocene. Geophysical Research Letters 35, L04709, doi: 10.1029/2007GL032027.

Bebermeier W., Holzkämper P., Meyer M., Schimpf S., Schütt B. (2018) Lateglacial to Late Holocene landscape history derived from floodplain sediments in context to prehistoric settlement sites of the southern foreland of the Harz Mountains, Germany, Quaternary International 463, 74-90, doi: 10.1016/j.quaint.2016.08.026.

Berry R.R., Chorley R.J. (2010) Atmosphere, Weather and Climate. Ninth Edition, Routledge.

Breitenbach S.F.M., Rehfeld K., Goswami B., Baldini J.U.L., Ridley H.E., Kennett D., Prufer K., Aquino V.V., Asmerom Y., Polyak V.J., Cheng H., Kurths J., Marwan N. (2012) COnstructing Proxy Records from Age models (COPRA). Climate of the Past 8, 1765–1779, doi: 10.5194/cp-8-1765-2012.

Breitenbach S.F.M., Lechleitner F.A., Meyer H., Diengdoh G., Mattey D., Marwan N. (2015) Cave ventilation and rainfall signals in dripwater in a monsoonal setting – a monitoring study from NE India. Chemical Geology 402, 111–124, doi: 10.1016/j.chemgeo.2015.03.011.

Büntgen U., Tegel W., Nicolussi K., McCormick M., Frank D., Trouet V., Kaplan J.O., Herzig F., Heussner K.-U., Wanner H., Luterbacher J., Esper J. (2011) 2500 Years of European Climate Variability and Human Susceptibility. Science 331, 578–582, doi: 10.1126/science.1197175.

Büntgen U., Myglan V.S., Charpentier Ljundqvist F., McCormick M., Di Cosmos N., Sigl M., Jungclaus J., Wagner S., Krusic P.J., Esper J., Kaplan J.O., de Vaan M.A.C., Luterbacher J., Wacker L., Tegel W., Kirdyanov A.V. (2016) Cooling and societal change during the Late Antique Little Ice Age from 536 to around 660 AD. Nature Geoscience 9, 231–236, doi: 10.1038/NGEO2652.

Brönnimann S. (2007) Impact of El Nino – Southern Oscillation on European Climate. Reviews of Geophysics 45, RG3003/2007, doi: 10.1029/2006RG000199.

Boch R., Spötl C., Kramers J. (2009) High-resolution isotope records of early Holocene rapid climate change from two coeval stalagmites of Katerloch Cave, Austria. Quaternary Science Reviews 28, 2527–2538, doi: 10.1016/j.quascirev.2009.05.015.

Boden AG (2006) Bodenkundliche Kartieranleitung (KA5), 5th ed., Schweitzerbart, Stuttgart.

Bowen G.J. (2008) Spatial analysis of the intra-annual variation of precipitation isotope ratios and its climatological corollaries. Journal of Geophysical Research 113, D05113, doi: 10.1029/2007JD009295

Cheng H., Edwards R.L., Hoff J., Gallup C.D., Richards D.A., Asmerom Y. (2000) The half-lives of uranium-234 and thorium-230. Chemical Geology 169, 17–33, doi: 10.1016/S0009-2541(99)00157-6.

Czymcik M., Dreibrodt S., Feeser I., Adolphi F., Brauer A. (2016) Mid-Holocene humid periods reconstructed from calcite varves of the Lake Woserin sediment record (north-eastern Germany). The Holocene 26, 935–946, doi: 10.1177/0959683615622549.

Comas-Bru L., McDermott F., Werner M. (2016) The effect of the East Atlantic pattern on the precipitation $\delta^{18}O$-NAO relationship in Europe. Journal of Climate Dynamics 47, 2059, doi: 10.1007/s00382-015-2950-1.

Cohen J., Saito K., Entekhabi D. (2001) The role of the Siberian high in Northern Hemisphere climate variability. Geophysical Research Letters 28, 299-302, doi: 10.1029/2000GL011927

Cohen J., Screen J.A., Furtado J.C., Barlow M., Whittleston D., Coumou D., Francis J., Dethloff K., Entekhabi D., Overland J., Jones J. (2014) Recent Arctic amplification and extreme mid-latitude weather. Nature Geoscience 7, 627-637, doi: 10.1038/NGEO2234

Connell W.E. and Patrick Jr. W.H. (1968) Effects of Redox Potential and pH. Science 159, 86-87. doi: 10.1016/S0045-6535(00)00492-6

Deininger M., Fohlmeister J., Scholz D., Mangini A. (2012) Isotope disequilibrium effects: The influence of evaporation and ventilation effects on the carbon and oxygen isotope composition of speleothems – A model approach. Geochimica et Cosmochimica Acta 96, 57-79, doi: 10.1016/j.gca.2012.08.013

Dorale J.A., Edwards L.R., Alexander Jr. E.C., Shen C.-C., Richards D.A., Cheng H. (2007) Uranium-series Dating of Speleothems: Current Techniques, Limits, & Applications. In: Sasowsky I.A. & Mylroie J. (eds.) Studies of Cave Sediments, Physical and Chemical Records of Paleoclimate. 177–197, doi: 10.1007/978-1-4419-9118-8_10.

Edwards P.J. (1998) Sulfur Cycling, Retention, and Mobility in Soils: A Review. Gen. Tech. Rep. NE-250. Radnor, PA: U. S. Department of Agriculture, Forest Service, Northeastern Research Station. 18 p.

Fairchild I.J. and Baker A. (2012) Speleothem Science. Wiley-Blackwell, 432 pg.

Fairchild I.J. and McMillan E.A. (2007) Speleothems as indicators of wet and dry periods. International Journal of Speleology 36, 69–74, doi: 10.5038/1827-806X.36.2.2.

Fairchild I.J. and Treble P.C. (2009) Trace elements in speleothems as recorders of environmental change. Quaternary Science Reviews 28, 449–468, doi: 10.1016/j.quascirev.2008.11.007.

Fohlmeister J., Schröder-Ritzrau A., Scholz D., Spötl C., Riechelmann D.F.C., Mudelsee M., Wackerbarth A., Gerdes A., Riechelmann S., Immenhauser A., Richter D.K., Mangini A. (2012) Bunker Cave stalagmites: an archive for central European Holocene climate variability. Climate of the Past 8, 1751–1764, doi: 10.5194/cp-8-1751-2012.

Fohlmeister J., Vollweiler N., Spötl C., Mangini A. (2013) COMNISPA II: Update of a mid-European isotope climate record, 11 ka to present. The Holocene 23, 749–754, doi: 10.1177/0959683612465446.

Frisia S., Borsato A., Spötl C., Villa I.M., Cucchi F. (2005a) Climate variability in the SE Alps of Italy over the past 17000 years reconstructed from a stalagmite record. Boreas 34, 445–455, doi: 10.1080/03009480500231336.

Frisia S., Borsato A., Fairchild I.J., Susini J. (2005b) Variations in atmospheric sulphate recorded in stalagmites by synchrotron micro-XRF and XANES analyses. Earth and Planetary Science Letters 235, 729–740, doi: 10.1016/j.epsl.2005.03.026.

Gascoyne M. (1992) Palaeoclimate determination from cave calcite deposits. Quaternary Science Reviews 11, 609–632, doi: 10.1016/0277-3791(92)90074-I.

Genty D. and Massault M. (1999) Carbon transfer dynamics from bomb-14C and d13C time series of a laminated stalagmite from SW France—Modelling and comparison with other stalagmite records. Geochimica et Cosmochimica Acta 63, 1537–1548, doi: 10.1016/S0016-7037(99)00122-2.

Genty D., Baker A., Massault M., Procter C., Gilmour M., Pons-Banchu E., Hamelin B. (2001) Dead carbon in stalagmites: carbonate bedrock paleodissolution vs. ageing of soil organic matter. Implications for ^{13}C variations in speleothems. Geochimica et Cosmochimica Acta 65, 3443–3457, doi: 10.1016/S0016-7037(01)00697-4.

Genty D., Blamart D., Ouahdi R., Gilmour M., Baker A., Jouzel J., Van-Exter S. (2003) Precise dating of Dansgaard–Oeschger climate oscillations in western Europe from stalagmite data. Nature 421, 833-837, doi: 10.1038/nature01391

Gibert L., Scott G. R., Scholz D., Budsky A., Ferrandez C., Martin R. A., Ribot F., Leria M. (2016) Chronology for the Cueva Victoria fossil site (SE Spain): Evidence for Early Pleistocene Afro-Iberian dispersals. Journal of Human Evolution 90, 183–197, doi: 10.1016/j.jhevol.2015.08.002.

Hahne J. (1991) Untersuchungen zur spät- und postglazialen Vegetationsentwicklung im nördlichen Bayern (Rhön, Grabfeld, Lange Berge). Flora 185, 17-32, doi: 10.1016/S0367-2530(17)32221-1.

Harris C., Arenson L.U., Christiansen H.H., Etzelmüller B., Frauenfelder R., Gruber S., Haeberli W., Hauck C., Hölzle M., Humlum O., Isaksen K., Kääb A., Kern-Lütschg M.A., Lehning M., Matsuoka N., Murton J.B., Nötzli J., Phillips M., Ross N., Seppälä M., Springman S.M., Vonder Mühll D. (2009) Permafrost and climate in Europe: Monitoring and modelling thermal, geomorphological and geotechnical responses. Earth-Science Reviews 92, 117–171, doi: 10.1016/j.earscirev.2008.12.002.

Haude W. (1954) Zur praktischen Bestimmung der aktuellen und potentiellen Evapotranspiration. Mitt Dtsch Wetterd. 8, 1–15.

Helama S., Meriläinen J., Tuomenvirta H. (2009) Multicentennial megadrought in northern Europe coincided with a global El Niño–Southern Oscillation drought pattern during the Medieval Climate Anomaly. Geology 37, 175-178, doi: 10.1130/G25329A.1.

Hendy C. (1971) The isotopic geochemistry of speleothems – The calculation of the effects of different modes of formation on the isotopic composition of speleothems and their applicability as palaeoclimatic indicators. Geochimica et Cosmochimica Acta 35, 801–824, doi: 10.1016/0016-7037(71)90127-X.

Hurrell J.W. (1995) Decadal trends in the North Atlantic Oscillation: Regional Temperatures and Precipitation. Science 269, 876–879, doi: 10.1126/science.269.5224.676.

Husson O. (2012) Redox potential (Eh) and pH as drivers of soil/plant/microorganism systems: A transdisciplinary overview pointing to integrative opportunities for agronomy. Plant and Soil 362, 389-417, doi: 10.1007/s11104-012-1429-7.

IAEA/WMO (2017) Global Network of Isotopes in Precipitation. The GNIP Database. Accessible at: http://www.iaea.org/water. Last access: 13.01.2019.

ILEK (2011) Chancen für die ländliche Entwicklung im Raum Schaumberger Land / Naturpark Thüringer Wald durch die touristische Erschließung der Bleßberghöhle. Integriertes Ländliches Entwicklungskonzept. Thüringer Landgesellschaft mbH, 108 pages.

James E.W., Banner J.L., Hardt B. (2015) A global model for cave ventilation and seasonal bias in speleothem paleoclimate records. Geochem. Geophys. Geosyst., 16, 1044–1051, doi: 10.1002/2014GC005658.

Kalis A.J., Merkt J., Wunderlich J. (2003) Environmental changes during the Holocene climatic optimum in central Europe - human impact and natural causes. Quaternary Science Reviews 22, 33–79, doi: 10.1016/S0277-3791(02)00181-6.

Kennett D.J., Breitenbach S.F.M., Aquino V.V., Asmerom Y., Awe J., Baldini J.U.L., Bartlein P., Culleton B.J., Ebert C., Jazwa C., Macri M.J., Marwan N., Polyak V., Prufer K.M., Ridley H.E., Sodemann H., Winterhalder B., Haug G.H. (2012) Development and Disintegration of Maya Political Systems in Response to Climate Change. Science 338, 788–791, doi: 10.1126/science.1226299.

Kottek M., Grieser J., Beck C., Rudolf B., Rubel F. (2006) World Map of the Köppen-Geiger climate classification updated. Meteorologische Zeitschrift 15, 259-263, doi: 10.1127/0941-2948/2006/0130.

Lachniet, M. S. (2009) Climatic and environmental controls on speleothem oxygen-isotope values. Quaternary Science Reviews 28, 412-432, doi: 10.1016/j.epsl.2009.05.010.

Lechleitner F.A., Baldini J.U.L., Breitenbach S.F.M., Fohlmeister J., McIntyre C., Goswami B., Jamieson R., van der Voort T., Prufer K., Marwan N., Culleton B., Kennett D., Asmerom Y., Eglinton T. (2016) High resolution radiocarbon Measurements in a tropical stalagmite reflect atmospheric ^{14}C and carbon cycle signals. Geochimica et Cosmochimica Acta 194, 233-252, doi: 10.1016/j.gca.2016.08.039.

Lechleitner F.A., Breitenbach S.F.M., Cheng H., Plessen B., Rehfeld K., Goswami B., Marwan N., Eroglu D., Adkins J.F., Haug G.H. (2017) Climatic and in-cave influences on $\delta^{18}O$ and $\delta^{13}C$ in a stalagmite from northeastern India through the last deglaciation. Quaternary Research 88, 458-471, doi: 10.1017/qua.2017.72.

Ludlow F., Stine A.R., Leahy P., Murphy E., Mayewski P.A., Taylor D., Killen J., Baillie M.G.L., Hennessy M., Kiely G. (2013) Medieval Irish chronicles reveal persistent volcanic forcing of severe winter cold events, 431–1649 CE. Environmental Research Letters 8, 024035, doi: 10.1088/1748-9326/8/2/024035.

Luetscher M. and Ziegler F. (2012) CORA-a dedicated device for carbon dioxide monitoring in cave environments. International Journal of Speleology 41, 273–281, doi: 10.5038/1827-806X.41.2.13.

Malkiewicz M., Waroszewski J., Bojko O., Egli M., Kabala C. (2016) Holocene vegetation history and soil development reflected in the lake sediments of the Karkonosze Mountains (Poland). The Holocene 26, 890-905, doi: 10.1177/0959683615622546.

Mangini A., Spötl C., Verdes P. (2005) Reconstruction of temperature in the Central Alps during the past 2000 yr from a $\delta^{18}O$ stalagmite record. Earth and Planetary Science Letters 235, 741–751, doi: 10.1016/j.epsl.2005.05.010.

Mangini A., Blumbach P., Verdes P. Spötl C., Scholz D., Machel H., Mahon S. (2007) Combined records from a stalagmite from Barbados and from lake sediments in Haiti reveal variable seasonality in the Caribbean between 6.7 and 3 ka BP. Quaternary Science Reviews 26, 1332–1343, doi: 10.1016/j.quascirev.2007.01.011.

Mann M., Rahmstorf S., Kornhuber K., Steinmann B.A., Miller S.K., Petri S., Coumou D. (2018) Projected changes in persistent extreme summer weather events: The role of quasi-resonant amplification. Science Advances 4: eaat3272, doi: 10.1126/sciadv.aat3272.

Martin-Puertas C., Matthes K., Brauer A., Muscheler R., Hansen F., Petrick C., Aldahan A., Possnert G., van Geel B. (2012) Regional atmospheric circulation shifts induced by a grand solar minimum. Nature Geoscience 5, 397–401, doi: 10.1038/NGEO1460.

Mayewski P.A., Meeker L.D., Twickler M.S., Whitlow S., Yang Q., Lyons W.B., Prentice M. (1997) Major features and forcing of high-latitude northern hemisphere atmospheric circulation using a 110,000-year long glaciochemical series. Journal of Geophysical Research 102, 26345–26366, doi: 10.1029/96JC03365.

Mayewski P.A., Rohling E.E., Stager E.C., Karle´n W., Maasch K.A., Meeker L.D., Meyerson E.A., Gasse F., van Kreveld S., Holmgren K., Lee-Thorp J., Rosqvist G., Rack F., Staubwasser M., Schneider R.R., Steig E.J. (2004) Holocene climate variability. Quaternary Research 62, 243–255, doi: 10.1016/j.yqres.2004.07.001.

McDermott F. (2004) Palaeo-climate reconstruction from stable isotope variations in speleothems: a review. Quaternary Science Reviews 23, 901–918, doi: 10.1016/j.quascirev.2003.06.021.

McDermott F., Atkinson T.C., Fairchild I.J., Baldini L.M., Mattey D.P. (2011) A first evaluation of the spatial gradients in $\delta^{18}O$ recorded by European Holocene speleothems. Global and Planetary Change 79, 275–287, doi: 10.1016/j.gloplacha.2011.01.005.

Mischel S.A., Scholz D., Spötl C. (2015) $\delta^{18}O$ values of cave drip water: a promising proxy for the reconstruction of the North Atlantic Oscillation? Climate Dynamics 45, 3035–3050, doi:

10.1007/s00382-015-2521-5.
Mischel S., Scholz D., Spötl C., Jochum K.P., Schröder-Ritzau A., Fiedler S. (2017) Holocene climate variability in central Germany and a potential link to the polar North Atlantic - a replicated record from three coeval speleothems. The Holocene 27, 509–525, doi: 10.1177/0959683616670246.
Meyer H., Schönicke L., Wand U., Hubberten H.W., Friedrichsen H. (2000) Isotope Studies of Hydrogen and Oxygen in Ground Ice – Experiences with the Equilibration Technique. Isotopes in Environmental and Health Studies 36, 133–149, doi: 10.1038/NGEO2349.
Mühlinghaus C., Scholz D., Mangini A. (2009) Modelling fractionation of stable isotopes in stalagmites. Geochimica et Cosmochimica Acta 73, 7275-7289, doi: 10.1016/j.gca.2009.09.010
Niggemann S., Mangini A., Mudelsee M., Richter D.K., Wurth G. (2003) Sub-Milankovitch climatic cycles in Holocene stalagmites from Sauerland, Germany. Earth and Planetary Science Letters 216, 539–547, doi: 10.1016/S0012-821X(03)00513-2.
Obert, J.C., Scholz, D., Felis, T., Brocas, W.M., Jochum, K.P., Andreae, M.O. (2016) ^{230}Th/U dating of Last Interglacial brain corals from Bonaire (southern Caribbean) using bulk and theca wall material. Geochimica et Cosmochimica Acta 178, 20–40, doi: 10.1016/j.gca.2016.01.011.
Olsen J., Anderson N.J. Knudsen M.F. (2012) Variability of the North Atlantic Oscillation over the past 5,200 years. Nature Geoscience 5, 808–812, doi: 10.1038/NGEO1589.
Peel M.C., Finlayson B.L., McMahon T.A. (2007) Updated world map of the Köppen-Geiger climate classification. Hydrol. Earth Syst. Sci. 11, 1633–1644, doi: 10.5194/hess-11-1633-2007.
Proctor C.J., Baker A., Barnes W.L., Gilmour M.A. (2000) A thousand year speleothem proxy record of North Atlantic climate from Scotland. Climate Dynamics 16, 815–820., doi: 10.1007/s0038200000.
Rehfeld K., Marwan N., Kurths J. (2011) Comparison of correlation analysis techniques for irregularly sampled time series. Nonlinear Processes in Geophysics 18, 389–404, doi: 10.5194/npg-18-389-2011.
Rehfeld K., Trachsel M., Telford R., Laepple T. (2016) Assessing performance and seasonal bias of pollen-based climate reconstructions in a perfect model world. Climate Past 12, 2255–2270, doi: 10.5194/cp-2016-13.
Reicherter K., Froitzheim N., Jarosinki M., Badura J., Franzke H.-J., Hansen M., Hübscher C., Müller R., Poprawa P., Reinecker J., Stackebrandt W., Voigt T., von Eynatten H., Zuchiewicz W. (2008): Alpine tectonics north of the Alps. In: McCann, T. (ed.): The geology of Central Europe. Geological Society (London), 1233-1285.
Reimer P.J., Bard E., Bayliss A., Beck J.W., Blackwell P.G., Bronk Ramsey C., Buck C.E., Cheng H., Edwards R.L., Friedrich M., Grootes P.M., Guilderson T.P., Haflidason H., Hajdas I.,

Hatté C., Heaton T.J., Hogg A.G., Hughen K.A., Kaiser K.F., Kromer B., Manning S.W., Niu M., Reimer R.W., Richards D.A., Scott E.M., Southon J.R., Turney C.S.M., van der Plicht J. (2013) IntCal13 and MARINE13 radiocarbon age calibration curves 0-50000 years calBP. Radiocarbon 55, 1869–1887, doi: 10.2458/azu_js_rc.55.16947.

Rheinwalt A., Boers N., Marwan N., Kurths J., Hoffmann P., Gerstengarbe F.-W., Werner P. (2016) Non‐linear time series analysis of precipitation events using regional climate networks for Germany. Climate Dynamics 46, 1065-1074, doi: 10.1007/s00382-015-2632-z.

Ridley H., Asmerom Y., Baldini J.U.L., Breitenbach S.F.M., Aquino V.V., Prufer K.M., Culleton B.J., Polyak V.J., Lechleitner F.A., Kennett D.J., Zhang M., Marwan N., Macpherson C.G., Baldini L.M., Xiao T., Awe J., Haug G.H. (2015) Aerosol forcing of the position of the intertropical convergence zone since AD 1550. Nature Geoscience 8, 195–200, doi: 10.1038/NGEO2353.

Riechelmann S., Schröder-Ritzrau A., Spötl C., Riechelmann D.F.C., Richter D.K., Mangini A., Frank N., Breitenbach S.F.M., Immenhauser A. (2017) Linking rain, soil and dripwaters at Bunker Cave: Insights into cave drip response and climate forcings from long-term monitoring. Chemical Geology 449, 194–205, doi: 10.1016/j.chemgeo.2016.12.015.

Russo E. and Cubasch U. (2016) Mid-to-late Holocene temperature evolution and atmospheric dynamics over Europe in regional model simulations. Climate of the Past 12, 1645–1662, doi: 10.5194/cp-12-1645-2016.

Saarni S., Saarinen T., Dulski P. (2016) Between the North Atlantic Oscillation and the Siberian High: A 4000-year snow accumulation history inferred from varved lake sediments in Finland. The Holocene 26, 423–431, doi: 10.1177/0959683615609747.

Scholz D., Frisia S., Borsato A., Spötl C., Fohlmeister J., Mudelsee M., Miorandi R., Mangini A. (2012) Holocene climate variability in north-eastern Italy: potential influence of the NAO and solar activity recorded by speleothem data. Climate of the Past 8, 1367–1383, doi: 10.5194/cp-8-1367-2012.

Seager R., Feldman J., Lis N., Ting M., Williams A.P., Nakamura J., Liu H., Henderson N. (2018) Whither the 100th Meridian? The Once and Future Physical and Human Geography of America's Arid–Humid Divide. Part II: The Meridian Moves East. Earth Interactions 22(5), 1-24, doi: 10.1175/EI-D-17-0012.1.

Seppä H., Bjune A.E., Telford R.J., Birks H.J.B., Veski S. (2009) Last nine-thousand years of temperature variability in Northern Europe. Climate of the Past 5, 523–535, doi: 10.5194/cp-5-523-2009.

Simonis D., Hense A., Litt T. (2012) Reconstruction of late Glacial and Early Holocene near surface temperature anomalies in Europe and their statistical interpretation. Quaternary International 274, 233–250, doi: 10.1016/j.quaint.2012.02.050.

Smith A., Wynn P.M., Barker P.A., Leng M.J., Noble S.R., Tych W. (2016) North Atlantic forcing of moisture delivery to Europe throughout the Holocene. Scientific Reports 6, 2445, doi:

10.1038/srep24745.

Thieblemont R., Matthes K., Omrani N.-E., Kodera K., Hansen F. (2015) Solar forcing synchronizes decadal North Atlantic climate variability. Nature Communications 6:8268, doi: 10.1038/ncomms9268.

Troester J.W. and White W.B. (1984) Seasonal fluctuations in the carbon dioxide partial pressure in a cave atmosphere. Water Resources Research 20, 153-156, doi: 10.1029/WR020i001p00153.

Trouet V., Esper J., Graham N.E., Baker A., Scourse J.D., Frank D. (2009) Persistent Positive North Atlantic Oscillation Mode Dominated the Medieval Climate Anomaly. Science 324, 78–80, doi: 10.1126/science.1166349.

Tan L., Cai Y., An Z., Cheng H., Shen C.-C., Breitenbach S., Gao Y., Edwards R., Zhang H., Du Y. (2015) A Chinese cave links climate change, social impacts, and human adaptation over the last 500 years. Scientific Reports 5:12284, doi: 10.1038/srep12284.

Vaks A., Bar-Matthews M., Matthews A., Ayalon A., Frumkin A. (2010) Middle-Late Quaternary paleoclimate of northern margins of the Saharan-Arabian Desert: reconstruction from speleothems of Negev Desert, Israel. Quaternary Science Reviews 29, 2647–2662, doi: 10.1016/j.quascirev.2010.06.014.

Vaks A., Gutareva O.S., Breitenbach S.F.M., Avirmed E., Mason A.J., Thomas A.L., Osinzev A.V., Kononov A.M., Henderson G.M. (2013) Speleothems reveal 500,000 year history of Siberian permafrost. Science 340, 183–186, doi: 10.1126/science.1228729.

Verheyden S., Keppens E., Fairchild I.J., McDermott F., Weis D. (2000) Mg, Sr and Sr isotope geochemistry of a Belgian Holocene speleothem: implications for paleoclimate reconstructions. Chemical Geology 169, 131–144, doi: 10.1016/S0009-2541(00)00299-0.

Vincent P.J., Lord T.C., Telfer M.W., Wilson P. (2011) Early Holocene loessic colluviation in northwest England: new evidence for the 8.2 ka event in the terrestrial record? Boreas 40, 105–115, doi: 10.1111/j.1502-3885.2010.00172.x.

von Grafenstein U., Erlenkeuser H., Brauer A., Jouzel J., Johnsen S.J. (1999) A Mid-European Decadal Isotope-Climate Record from 15,500 to 5000 Years B.P. Science 284, 1654–1657, doi: 10.1126/science.284.5420.1654.

Wackerbarth A. K., Scholz D., Fohlmeister J., Mangini A. (2010) Modelling the $\delta^{18}O$ value of cave drip water and speleothem calcite. Earth and Planetary Science Letters 299, 387–397, doi: 10.1016/j.epsl.2010.09.019.

Wolff C., Plessen B., Dudashvili A., Breitenbach S.F.M., Cheng H., Edwards R.L., Strecker M. (2017) Precipitation evolution of Central Asia during the last 5000 years. The Holocene 27, 142–154, doi: 10.1177/0959683616652711.

Wong C.I. and Breeker D.O. (2015) Advancements in the use of speleothems as climate archives. Quaternary Science Reviews 127, 1–18, doi: 10.1016/j.quascirev.2015.07.019.

Woolings T. and Blackburn M. (2012) The North Atlantic Jet Stream under Climate Change and Its

Relation to the NAO and EA Patterns. Journal of Climate 25, 886-902, doi: 10.1175/JCLI-D-11-00087.1.

Wynn P.M., Fairchild I.J., Frisia S., Spötl C., Baker A., Borsato A., EIMF (2010) High-resolution sulphur isotope analysis of speleothem carbonate by secondary ionisation mass spectrometry. Chemical Geology 271, 101–107, doi: 10.1016/j.chemgeo.2010.01.001.

Yang, Q., Scholz, D., Jochum, K. P., Hoffmann, D. L., Stoll, B., Weis, U., Schwager, B., Andreae, M. O. (2015) Lead isotope variability in speleothems – A promising new proxy for hydrological change? First results from a stalagmite from western Germany. Chemical Geology 396, 143–151, doi: 10.1016/j.chemgeo.2014.12.028.